Cerebellar Contribution to Preparatory Activity in Motor Neocortex

Highlights

- Similar activity in dentate nucleus (DN) and ALM cortex prior to reward acquisition

- Silencing DN activity selectively suppresses preparatory activity in ALM

- Preparatory activity likely controlled by learned decrease in Purkinje cell firing

- Dynamics of preparatory activity imply reward time prediction from external cues

Authors

Francois P. Chabrol, Antonin Blot, Thomas D. Mrsic-Flogel

Correspondence

t.mrsic-flogel@ucl.ac.uk

In Brief

Chabrol et al. show that the cerebellum is directly involved in maintaining preparatory activity in the premotor neocortex during learned, goal-directed behavior. Their results suggest the cerebellum provides a learned timing signal required for motor preparation in the neocortex.

Neuron

Article

CellPress

Cerebellar Contribution to Preparatory Activity in Motor Neocortex

Francois P. Chabrol,[1,2] Antonin Blot,[1,2] and Thomas D. Mrsic-Flogel[1,2,3,*]
[1]Biozentrum, University of Basel, Klingelbergstrasse 70, 4056 Basel, Switzerland
[2]Sainsbury Wellcome Center, University College London, 25 Howland Street, London W1T 4JG, UK
[3]Lead Contact
*Correspondence: t.mrsic-flogel@ucl.ac.uk
https://doi.org/10.1016/j.neuron.2019.05.022

SUMMARY

In motor neocortex, preparatory activity predictive of specific movements is maintained by a positive feedback loop with the thalamus. Motor thalamus receives excitatory input from the cerebellum, which learns to generate predictive signals for motor control. The contribution of this pathway to neocortical preparatory signals remains poorly understood. Here, we show that, in a virtual reality conditioning task, cerebellar output neurons in the dentate nucleus exhibit preparatory activity similar to that in anterolateral motor cortex prior to reward acquisition. Silencing activity in dentate nucleus by photoactivating inhibitory Purkinje cells in the cerebellar cortex caused robust, short-latency suppression of preparatory activity in anterolateral motor cortex. Our results suggest that preparatory activity is controlled by a learned decrease of Purkinje cell firing in advance of reward under supervision of climbing fiber inputs signaling reward delivery. Thus, cerebellar computations exert a powerful influence on preparatory activity in motor neocortex.

INTRODUCTION

Persistent firing, a hallmark of cortical activity in frontal areas of the neocortex (Funahashi et al., 1989; Fuster and Alexander, 1971; Li et al., 2015; Tanji and Evarts, 1976; Wise, 1985), links past events to future actions. In the motor-related areas of the neocortex, the persistent activity that emerges prior to movement is often referred to as preparatory activity (Churchland et al., 2006; Kubota and Hamada, 1979; Paz et al., 2003; Wise, 1985), but the circuit mechanisms underlying the origin, timing, and control of this activity remain unclear. A positive thalamic feedback loop has been shown to be involved in the maintenance of preparatory signals in anterolateral motor (ALM) neocortex of mice (Guo et al., 2017), raising the possibility that extra-cortical inputs might regulate neocortical activity in advance of goal-directed movements (Kopec et al., 2015; Ohmae et al., 2017; Tanaka, 2007) via the thalamus. A prominent extra-cortical input to the motor thalamus is provided by the cerebellum (Guo et al., 2017; Ichinohe et al., 2000; Middleton and

Strick, 1997; Thach and Jones, 1979), a key brain structure for the learning of sensorimotor and internal contexts relevant for movement timing (Mauk and Buonomano, 2004). The cerebellum is therefore a plausible candidate for participating in the computation of preparatory activity.

The cerebellum is bidirectionally connected with the neocortex via the disynaptic cerebello-thalamo-cortical and cortico-ponto-cerebellar pathways (Jörntell and Ekerot, 1999; Leergaard et al., 2006; Lu et al., 2007; Proville et al., 2014; Suzuki et al., 2012). The sole output of the cerebellum is the deep cerebellar nuclei (DCN), where axon terminals from ∼40 inhibitory Purkinje cells converge on individual postsynaptic neurons (Person and Raman, 2011). The dentate (DN), interpositus (IPN), and fastigial (FN) subdivisions of the deep cerebellar nuclei send excitatory projections to the motor thalamic regions linked to cortical areas involved in the preparation and execution of voluntary movements (Angaut and Bowsher, 1970; Gao et al., 2018; Hoover and Vertes, 2007; Ichinohe et al., 2000; Kelly and Strick, 2003; McCrea et al., 1978; Middleton and Strick, 1997; Sawyer et al., 1994; Shinoda et al., 1985; Thach and Jones, 1979). Although the cerebellum is mostly known for its role in rapid adjustments in the timing and degree of muscle activation, neurons at different stages of the cerebellar hierarchy can also represent signals related to upcoming movements or salient events, such as reward (Giovannucci et al., 2017; Huang et al., 2013; Kennedy et al., 2014; Wagner et al., 2017). For instance, DN neurons exhibit ramping activity predictive of the timing and direction of self-initiated saccades (Ashmore and Sommer, 2013; Ohmae et al., 2017). Moreover, inactivation of IPN activity reduces persistent activity in a region of medial prefrontal cortex involved in trace eyeblink conditioning (Siegel and Mauk, 2013). Finally, a recent study has established the existence of a loop between ALM and the cerebellum necessary for the maintenance of preparatory activity (Gao et al., 2018). These results suggest that the cerebellum participates in programming future actions, but the details of how it may contribute to preparatory activity in the neocortex during goal-directed behavior remain to be determined.

RESULTS

Preparatory Activity in ALM prior to Reward Acquisition in a Virtual Corridor

We developed a visuomotor task in which mice ran through a virtual corridor comprising salient visual cues to reach a defined
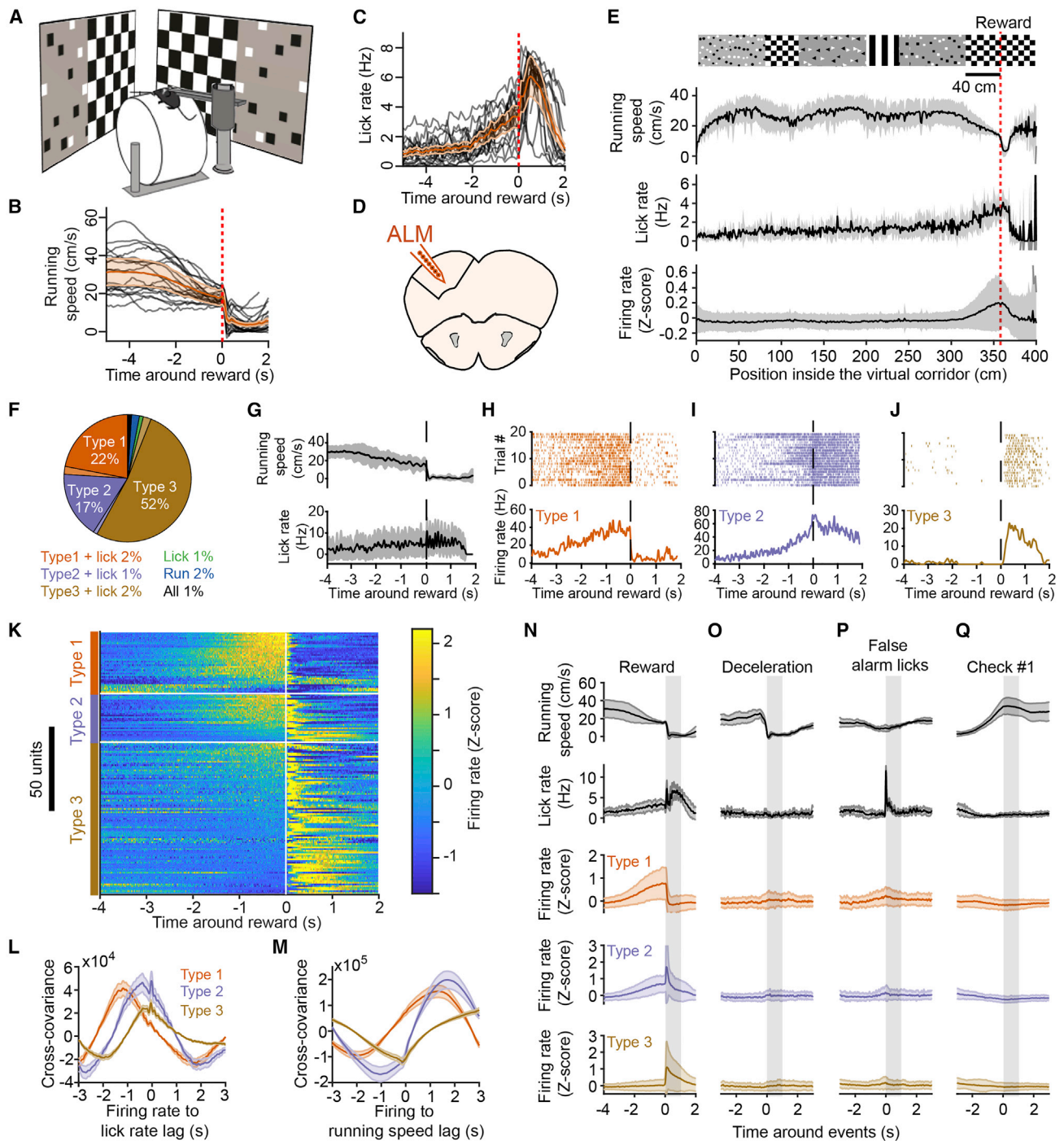
Figure 1. Preparatory Activity in the Anterolateral Motor Cortex

(A) Schematic of the virtual reality setup.

(B) Running speed profiles for all mice from Figures 1 and 2 (black curves, 21 expert mice) and population average (orange trace, shading is SD). Red vertical dashed line indicates reward.

(C) Same as (B) but for lick rate.

(D) Schematic showing recording location in the anterolateral motor cortex (ALM).

(E) (From top to bottom) Structure of visual textures lining the virtual corridor walls with the red dotted line indicating the position of reward delivery 40 cm from the appearance of the checkerboard pattern (scale bar), average (black line) and SD (shaded area) of running speed, lick rate, and Z-scored firing rate of all ALM neurons exhibiting task modulation, as a function of position in the virtual corridor. The visual patterns are aligned to the position at which they fully appear in the field of view of the mice (i.e., when they reach the back edge of the monitors).

(legend continued on next page)

location where a reward was delivered (40 cm from the appearance of the second checkerboard pattern; Figure 1A; see STAR Methods). Within a week of training, mice learned to estimate the reward location from visual cues and adjusted their behavior accordingly by running speedily through the corridor before decelerating abruptly and often licking in anticipation of reward delivery (Figures 1B, 1C, and S1A–S1C). This behavioral progress was apparent during the recording session, as the number of false alarm licks outside of the reward zone decreased within tens of trials (Figure S1B), and deceleration and lick onsets emerged in anticipation of reward (Figure S1C).

We used silicon probes to record the spiking of neurons in ALM neocortex (Figure 1D) to determine how their activity was modulated during our behavioral task, especially during the transition period between running and licking around reward delivery. We found that the activity of task-modulated ALM neurons (n = 169, 6 mice; see below) remained, on average, at baseline levels during the entire trial except in the rewarded section of the corridor, where it substantially increased (Figure 1E). We identified the neural correlates of running, licking, or reward context by applying a generalized linear model (GLM) (Park et al., 2014) to classify ALM neurons according to running speed, lick times, and reward times (Figure S2; see STAR Methods). The activity of 49% of putative ALM pyramidal neurons (see STAR Methods) was modulated by these task variables (n = 169/343, 6 mice). The activity of 91% of those units was related to reward times, and that of the remaining units was modulated by running, licks, or a combination of these behavioral variables and reward times (Figure 1F). All neuron classes included a minority of units exhibiting decrease rather than increase in activity. The population modulated by reward times included neurons with activity starting a few seconds before reward delivery (referred to as "preparatory activity") and terminating abruptly thereafter (classified as "type 1"; see Svoboda and Li, 2018; n = 37, 33 with increasing and 4 with decreasing activity; Figures 1G, 1H, and 1K), neurons active before and after reward delivery ("type 2"; n = 29, 20 with activity increasing before and after reward, 7 with activity decreasing before and increasing after reward, and 2 with activity increasing before and decreasing after reward; Figures 1I and 1K), or neurons active after reward delivery ("type 3"; n = 88, 79 with increasing and 9 with decreasing activity; Figures 1J and 1K), consistent with ALM activity observed during a delayed licking task in mice (Svo-

boda and Li, 2018). Accordingly, ALM population activity tiled the period around reward acquisition (Figure 1K). Cross-covariance analysis between firing rate and lick rate revealed that preparatory activity arises long before the time of the reward (Figure 1L). Type 1–3 neuronal activity in ALM preceded lick rate by 1,188, 383, and 350 ms (peaks of mean cross-covariances), respectively, on average. Moreover, type 1 and 2 neuronal activity preceded running speed changes (Figure 1M), albeit with anti-correlation, by 1,961 ms and 1,045 ms on average, respectively.

To verify that the activity of type 1–3 ALM neurons was specific to reward context (Figure 1N), we examined whether their firing was related to changes in motor output or visual input outside of the rewarded corridor location. Specifically, their activity was not modulated by deceleration events (Figure 1O) or licking bouts outside of the reward zone (Figure 1P) nor by the appearance of non-rewarded checkerboards in a different segment of the virtual corridor (Figure 1Q). These results confirm that the activity of type 1 and 2 ALM neurons before reward acquisition does not reflect motor action or sensory input per se but instead is consistent with preparatory activity building up in anticipation of licking for reward, as described previously (Guo et al., 2014; Li et al., 2015). We noticed that mice consistently decelerated after the appearance of the non-rewarded checkerboard, although they did not produce substantially more licks on average at this corridor position (Figures 1E and S3A). To verify whether we could see any correlate of this behavior in ALM activity (Figure S3B), we plotted the activity of type 1–3 neurons as a function of distance in the corridor (Figure S3C). Type 1–3 neurons were selectively active around the position of reward delivery, showing very little modulation of activity around the non-rewarded checkerboard (Figures S3C and S3D).

The Cerebellar Dentate Nucleus Exhibits Preparatory Activity

Because the DN sends excitatory projections to the motor thalamus (Gao et al., 2018; Ichinohe et al., 2000; Middleton and Strick, 1997; Thach and Jones, 1979), which has been shown to participate in the maintenance of preparatory activity in mouse ALM neocortex (Guo et al., 2017), we investigated whether DN activity could influence ALM processing. We first recorded the activity of DN neurons to determine how their activity was modulated during the task (Figure 2A). Forty-four percent of all recorded DN neurons (n = 355, 15 mice) could be classified

(F) Summary ALM neuron classification (n = 169 neurons, 6 mice).

(G) Running speed (top) and lick rate (bottom) around reward time for an example recording. Black line is the average; gray shaded area is the SD.

(H–J) Spiking activity from example neurons in ALM, classified as type 1 (H), type 2 (I), and type 3 (J) from the same recording as in (G). (Top) Spike raster for 20 consecutive trials is shown. (Bottom) Average response profile centered on reward delivery is shown from the same trials shown above. The vertical dotted lines across (G)–(J) indicate reward time.

(K) Mean Z-scored firing rate of reward-time-modulated ALM neurons centered on reward time represented by the white vertical line. Within types, neurons (one per line) are sorted by their mean Z score value in the last second before reward.

(L) Average cross-covariance between firing rates of all neurons (grouped by type) and lick rate for −2- to 2-s time lags (10-ms binning). The shaded areas represent SEM.

(M) Cross-covariance between firing rates and running speed, description as in (L).

(N) Average (line) and SD (shaded area) centered on reward delivery (vertical shaded area represents time window from reward to reward + 1 s) for, from top to bottom, running speed, lick rate, and firing rate (Z scored), averaged for all type 1, type 2, and type 3 neurons.

(O–Q) Same as in (N) for responses centered on deceleration events outside of the reward zone (O), first lick of a train outside of the reward zone (P), and the appearance of the first non-rewarded checkerboard visual stimulus (Q) at the front edge of the monitors (see Figure S3).
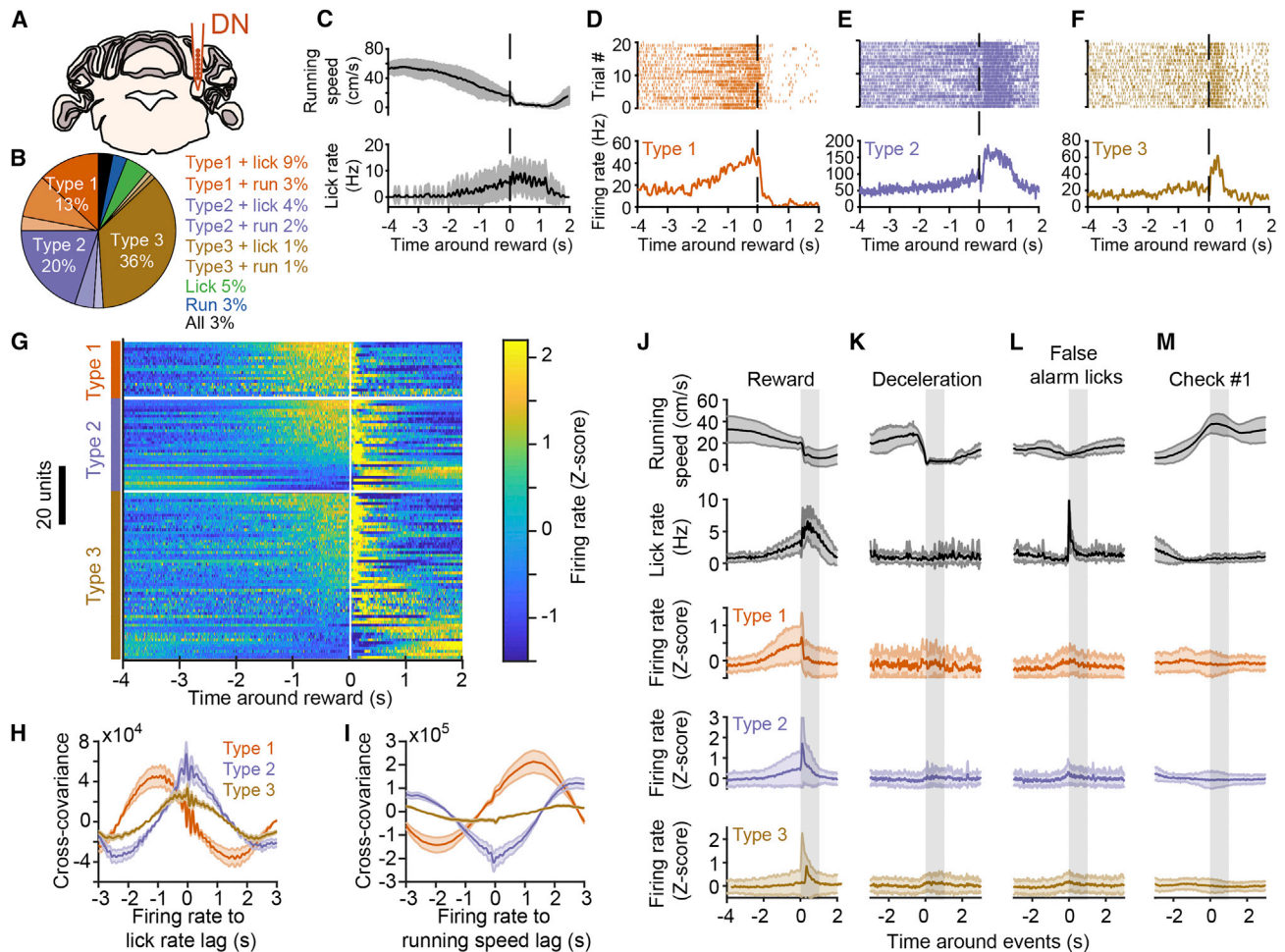
Figure 2. Preparatory Activity in the Dentate Nucleus

(A) Schematic showing recording location in the dentate nucleus (DN).

(B) Summary DN neuron classification (n = 156 neurons, 15 mice).

(C) Running speed (top) and lick rate (bottom) around reward time for an example recording. Black line is the average; gray shaded area is the SD.

(D–F) Spiking activity from example neurons in DN, classified as type 1 (D), type 2 (E), and type 3 (F; same recording as in C). (Top) Spike raster for 20 consecutive trials is shown. (Bottom) Average response profile centered on reward delivery is shown from the same trials shown above. The vertical dotted lines across (C)–(F) indicate reward time.

(G) Mean Z-scored firing rate of reward-time-modulated DN neurons centered on reward time (white vertical line). Within types, neurons (one per line) are sorted by their mean Z score value in the last second before reward.

(H) Average cross-covariance between firing rates of all neurons (grouped by type) and lick rate for −2- to 2-s time lags (10-ms binning). The shaded areas represent SEM.

(I) Cross-covariance between firing rates and running speed, description as in (H).

(J) Average (line) and SD (shaded area) centered on reward delivery (vertical shaded area represents time window from reward to reward + 1 s) for, from top to bottom, running speed, lick rate, and firing rate (Z scored), averaged for all type 1, type 2, and type 3 neurons.

(K–M) Same as in (J) for responses centered on deceleration events outside of the reward zone (K), first lick of a train outside of the reward zone (L), and the appearance of the first non-rewarded checkerboard visual stimulus (M) at the front edge of the monitors (see Figure S3).

according to our task variables, and the activity of 69% of classified DN neurons was related to reward times only (Figure 2B). The activity of the other neurons was related to lick times, running, or a mixture of these variables plus reward times (Figure 2B). Of neurons whose activity was modulated by reward times only, 13% were classified as type 1 (n = 20, 18 with increasing and 2 with decreasing activity), 20% as type 2 (n = 32, 22 with activity increasing before and after reward, 9

with activity decreasing before and increasing after reward, and 1 with activity increasing before and decreasing after reward), and 36% as type 3 neurons (n = 57, 51 with increasing and 6 with decreasing activity; Figures 2B–2G). As in ALM, type 1–3 neuronal activity tiled the period around reward delivery (Figure 2G). Type 1–3 neurons' spiking preceded lick rate by 915, 50, and 10 ms (peaks of mean cross-covariances), respectively, on average (Figure 2H). Moreover, type 1 DN neuron activity was
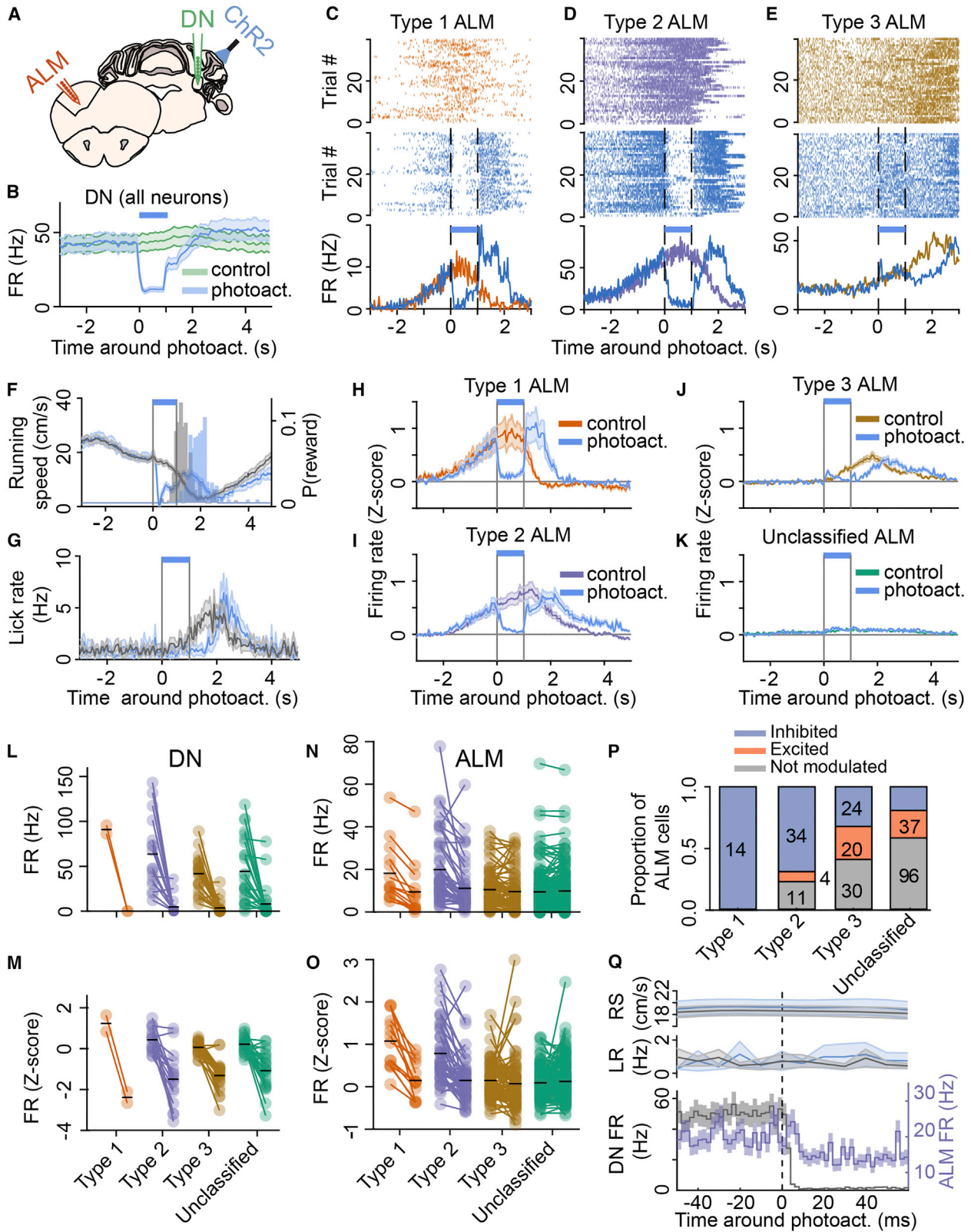
(legend on next page)

anti-correlated with running speed and preceded its changes by 1,972 ms on average (Figure 2I). Type 2 and 3 DN neuronal activity emerged less in advance of behavioral changes on average compared to ALM (Figures 1L and 1M), although the distribution of cross-covariance peak times was not significantly different between ALM and DN neurons (p > 0.05; Wilcoxon signed-rank test). As in ALM, the activity of type 1–3 DN neurons was not modulated by changes in motor behavior or visual input (Figures 2K–2M) but specifically emerged around the position of reward delivery (Figures 2J and S3E–S3G). Thus, preparatory activity in DN (type 1 neurons) was largely indistinguishable from that recorded in ALM. Type 2 and 3 DN neuronal populations, on the other hand, seemed to be more closely related to behavioral changes than their counterparts in ALM (see cross-covariance plots in Figures 2H and 2I versus Figures 1L and 1M). To test whether preparatory activity is somewhat specific to DN or can also be found in other deep cerebellar nuclei, we recorded from the IPN (Figure S4C), located more medially than the DN (Figure S4A), which also projects to the motor thalamus (Guo et al., 2017). We found a lower proportion of neurons classified as type 1 (1/74 classified neurons, 5 mice) and type 2 (8/74) in the IPN compared to DN, although this difference was only significant for type 1 neurons (Figures S4B and S4D–S4F). On the other hand, type 3 neurons were more enriched in the IPN (54/74 classified neurons) than in the DN population (Figures S4B and S4D–S4F). Hence, preparatory activity appears to be more represented in the DN.

DN Contributes to ALM Preparatory Activity
To determine the contribution of DN firing on ALM preparatory activity, we silenced DN output by photoactivating cerebellar Purkinje cells (PCs) expressing channelrhodopsin-2 under the control of the specific Purkinje cell protein (PCP2) promoter (Figure 3A; see STAR Methods). Because in our behavioral task reward delivery is dependent on visuomotor context, we targeted the photoactivation to the lateral part of crus 1 in the cerebellar cortex, a region that projects to DN (Payne, 1983; Voogd, 2014) and uniquely responds to electrical stimulation of both visual and motor cortex (Figure S5), suggesting it integrates visuomotor signals from the neocortex. The activation of PCs in lateral crus 1 began 20 cm in advance of the rewarded position in the virtual corridor (Figure 1E) and lasted 1 s in order to terminate around reward delivery. Simultaneous silicon probe recordings from DN and ALM (Figure 3A) revealed that optogenetic activation of PCs effectively silenced most DN neurons (Figures 3B and S6A) regardless of response type (Figures 3L and 3M; firing rate control versus PC photoactivation: 49.7 ± 33.4 Hz versus 4.1 ± 10 Hz; 92% decrease; p < 0.0001; n = 69, 3 mice), consequently resulting in a substantial reduction of activity in a large fraction of ALM neurons (n = 98/279, 5 mice; Figures 3C–3K and S6B). Activity of all type 1 and most type 2 ALM neurons was robustly suppressed by PC photoactivation (respectively, 14/14 and 34/49 neurons; Figures 3N–3P), such that, on average, their firing rate decreased to baseline activity levels (type 1 control: 18.5 ± 14 Hz versus photoactivation: 9.8 ± 12.7 Hz, n = 14, p = 0.0001; type 2 control: 20.3 ± 16.1 Hz versus photoactivation: 11.5 ± 11.7 Hz, n = 49, p < 0.0001; Figures 3H, 3I, 3N, and 3O). Type 3 and unclassified ALM neurons exhibited a mixture of effects, including a fraction of units that were excited (Figures 3E and 3P), and their population activity during PC photoactivation was not affected on average (respectively, 10.8 ± 8.9 Hz versus 9.9 ± 9.3 Hz, p = 0.09, n = 74 and 9.8 ± 9.8 Hz versus 10.2 ± 10.3 Hz, p = 0.89, n = 165; Figures 3J, 3K, 3N, and 3O). Type 1 and 2 neurons were significantly more inhibited during photoactivation (Figure S7A) and had higher firing rates (Figure S7B) than type 3 and unclassified neurons. The effect of photoactivation did not seem to be explained by the difference of firing rate between neuron types (Figures S7C–S7F) and, even when excluding neurons with low firing rate (below 10 Hz), only type 1 and type 2 neurons were significantly affected by photoactivation (Figure S7G). Furthermore, the amplitude of the effect of PC photoactivation appeared to be dependent on the size of the ramp (as defined in Figure S7H) and not on the firing rate in control condition (Figure S7I). Indeed, in a linear model, including ramp size and control firing rate (see STAR Methods), the photoactivation effect was proportional to the ramp size and not to the

Figure 3. Cerebellar Output Is Required for the Persistence of ALM Preparatory Activity
(A) Schematic of experiments. The dentate nucleus (DN, green) and anterolateral motor cortex (ALM, orange) were simultaneously recorded in L7-ChR2 mice performing the task during photoactivation of Purkinje cells (PCs) in lateral crus 1 (ChR2, blue light).
(B) PC photoactivation effectively silenced DN population activity. Duration of photoactivation is indicated by a blue bar.
(C–E) Spike raster during control trials (top) and photoactivation trials (middle) and average responses (bottom) from example neurons recorded in ALM classified as type 1 (C), type 2 (D), or type 3 (E) around the photoactivation period (vertical dashed lines and blue bar).
(F and G) Average profiles aligned to photoactivation onset in photoactivation trials (blue traces, average and SD) and control trials (gray) for running speed (F) and lick rate (G) and distribution of reward probability (P(reward)) in photoactivation trials (F, blue histogram) and control trials (F, gray histogram).
(H–K) Response profiles of ALM neurons aligned to photoactivation onset for type 1 (H), type 2 (I), type 3 (J), and unclassified cells (K) during photoactivation (blue traces, average and SD) and control trials (colored traces).
(L–O) Quantification of photoactivation effect. Average firing rate (L and N) and Z-scored firing rate (M and O) during the first second after photoactivation onset for DN neurons (L and M) and ALM neurons (N and O). For all plots, the first column of dots (1 per neuron) is the control condition and the second column the photoactivation condition. The black lines indicate the population mean.
(P) Proportion of cells being inhibited (blue), excited (orange), or not significantly modulated (gray) for the 4 classes of ALM neurons (number of neurons indicated in each bar, except for excited type 2 neurons, where it is shown on the right side of the bar).
(Q) (Bottom) Average response profiles of firing rate for all DN neurons (gray) and all type 1 and type 2 ALM neurons (purple) with significant reduction in activity compared to control trials (2-ms binning; see STAR Methods), aligned to PC photoactivation onset (vertical dotted line). Traces with shaded areas are mean ± SEM. (Top) Running speed (RS) and lick rate (LR) did not change in this time window and were not significantly different between control (black, average and SD) and photoactivation (blue) trials.
(L–Q) Data shown in those panels include an additional recording (6 recordings in total, 5 mice) where the photoactivation period lasted 2 s (versus 1 s in all other recordings).

CellPress

firing rate (p < 1e−5 versus p = 0.7). Therefore, lateral crus 1 PC photoactivation preferentially impacted ALM neurons whose activity was modulated in anticipation of reward.

In trials with PC photoactivation, mice transiently ceased to run approximately 170 ms after light onset (Figures 3F, curve, and S6C), reaching the reward later (Figure 3F, histograms) and licking at that time (Figure 3G). This effect on running is reminiscent of dystonic postures that have been previously observed during cerebellar deficits or pharmacological activations (Shakkottai, 2014) and prevents any interpretation of the effect of PCs photoactivation on preparatory behavior. As type 3 neurons were modulated after the reward, their firing peaked later in photoactivation trials (Figure 3J) but remained aligned to reward delivery (Figure S8). However, the suppression of neuronal activity in DN and ALM was not a consequence of running speed change because the onset of the firing rate decrease was almost immediate in DN neurons (2 ms; see STAR Methods) and was 10 ms for type 1 and 2 ALM neurons (Figure 3Q), and a significant decrease in ALM activity during PC photoactivation was observed before any change in running speed (10–150 ms after photoactivation onset; type 1 control: 18.3 ± 14.5 Hz versus photoactivation: 10.2 ± 14.1, n = 14, p = 0.0017; type 2 control: 19.19 ± 15.8 Hz versus photoactivation: 14.6 ± 16.2, n = 49, p = 0.0002; control running speed: 18.7 ± 7.5 cm/s versus photoactivation 18.9 ± 6.3, p = 0.84). The short-latency decrease in ALM activity by PC photoactivation (8 ms, accounting for the delay in DN inhibition) was consistent with the time delay expected for the withdrawal of excitation via the disynaptic pathway from DN to ALM via the thalamus. Type 3 ALM neurons that were inhibited exhibited a similar time profile than type 1 or 2 neurons, with a significant drop in activity 8 ms after PC photoactivation onset (Figure S6D). On the other hand, excited type 3 neurons exhibited significant changes in activity only after 40 ms (Figure S6E), suggesting the involvement of an additional, possibly intracortical, circuit. These results demonstrate that the maintenance of preparatory activity in ALM requires short-latency, excitatory drive from the cerebellum.

Preparatory activity recovered in ALM shortly after the end of PC photoactivation (Figures 3H and 3I), which suggests the involvement of other brain regions in its maintenance. We tested whether the contralateral cerebellar-cortical circuit, which should remain unaffected during unilateral photoactivation, reinstated ALM activity by photoactivating lateral crus 1 PCs on both sides (Figure S9A). Moreover, we established a progressive ramp in the offset of the laser to avoid activity rebound in the DCN (Figure S9B; see STAR Methods). We found no difference in the effect of unilateral versus bilateral PC photoactivation on type 1 (n = 10, 8 inhibited, 3 mice), type 2 (n = 13, 10 inhibited), or type 3 ALM neurons (n = 33, 18 inhibited, 11 excited; Figure S9B), except for shorter latency of inhibition upon unilateral photoactivation (8 ms versus 14 ms for bilateral photoactivation; Figure S9C). These data suggest that other brain regions involved in motor preparation, such as the basal ganglia (Kunimatsu et al., 2018), may contribute to the recovery of preparatory activity.

Finally, we tested the role of other deep cerebellar nuclei toward preparatory activity during our task. In contrast to DN, the activity of neurons in IPN was modulated more after reward

delivery than before, with fewer neurons exhibiting preparatory activity in anticipation of reward acquisition (Figure S4). Moreover, by photoactivating PCs in lobule IV-V (Figure S10A), which exclusively inhibits neurons in the FN (Voogd, 2014), we observed a strong suppression of type 1 (n = 9/10, 3 mice) and type 2 ALM neurons (n = 11/15) but with a substantially longer latency than upon lateral crus 1 PC photoactivation (Figures S10B and S10C). In contrast to the very short latency suppression following lateral crus 1 photoactivation (10 ms; Figure 3), the first significant reduction in type 1 or 2 ALM during lobule IV-V PC photoactivation occurred after 280 ms (Figure S10D), a delay too long to result from a direct connection from FN to the motor thalamus. Both lateral crus 1 and lobule IV-V PC photoactivation induced a sharp deceleration in mouse running (at 165 and 210 ms, respectively); however, unlike for lateral crus 1 PC photoactivation, the behavioral effect during lobule IV-V PC photoactivation preceded the inhibition of type 1 or 2 ALM neuronal activity, suggesting that the latter resulted from the mouse arrest. Additionally, type 3 ALM neurons appeared more excited upon lobule IV-V PC photoactivation (Figure S10C) but with a similar time profile than with lateral crus 1 PC photoactivation (50-ms onset), indicating that this excitatory effect on ALM activity and the inhibition of running behavior are not specific to the DN-ALM circuit. Taken together, our results suggest the existence of a dedicated DN output participating in preparatory activity.

Reward-Time-Based PC Learning in Lateral Crus 1 as a Likely Mechanism for Setting the Timing of Preparatory Activity

To gain insight in how preparatory activity could emerge in DN neurons that are under the inhibitory control of the cerebellar cortex, we recorded simultaneously from putative PCs in lateral crus 1 (Figures S11A–S11F; see STAR Methods) and from DN neurons (n = 3 mice; Figures 4A and 4B). The firing of PCs was modulated on the same timescale around the time of reward delivery as simultaneously recorded DN neurons (Figures 4C–4H). Many PCs exhibited inverse modulation of activity compared to DN neurons, resulting in negative cross-covariances between simultaneously recorded PC-DN pairs (Figure 4I; see STAR Methods), consistent with the fact that PCs provide inhibitory input onto DN neurons. Most PCs ramped down their activity prior to reward (Figure 4K), and DN neurons exhibited either activity increases or decreases (Figure 4J). On average, PCs decreased their firing in the second preceding reward (−0.14 ± 0.41; mean Z-scored firing rate and SD; n = 56; p = 0.0005), in contrast to DN neurons (0.06 ± 0.54; n = 69; p = 0.4; PC versus DN: p = 0.003; Figure 4L). To verify whether this PC activity profile is specific to lateral crus 1, we recorded from the adjacent crus 2 (Figure S12), a cerebellar cortical region which also projects to the DN. We found that crus 2 PCs mostly exhibited decreases in activity after reward (Figures S12E and S12F), pre-reward decrease in activity being significantly less apparent than in crus 1 (Figure S12G). To test whether the recorded regions of crus 1 and DN were functionally connected, we computed the cross-correlogram between all pairs of simultaneously recorded neurons. A small fraction of these correlograms were modulated (46/1,855; see STAR Methods;

CellPress
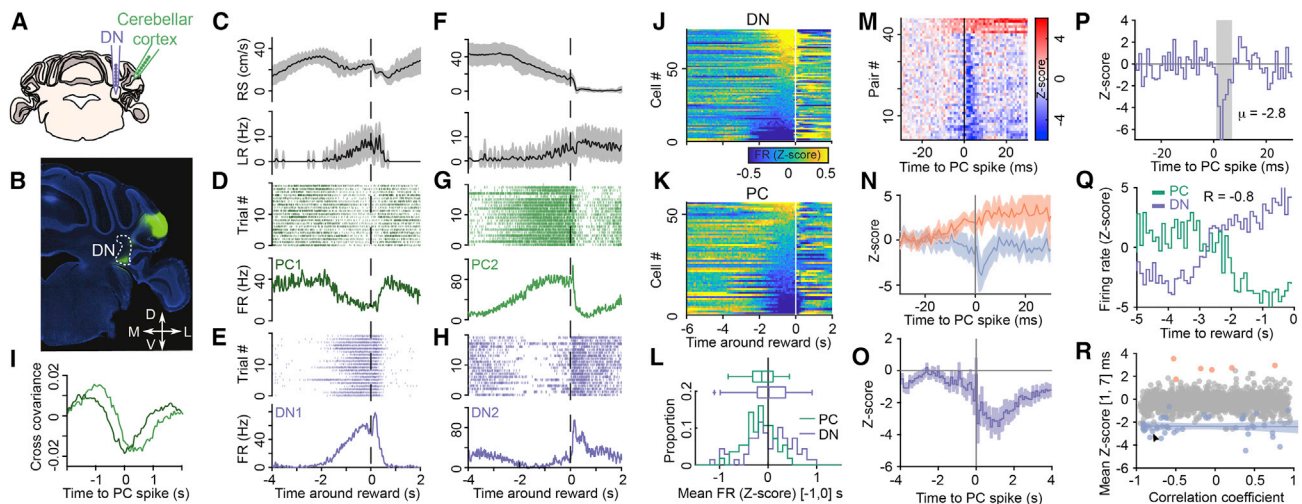
Figure 4. The Relationship between Activity of Lateral Crus 1 Purkinje Cells and Dentate Nucleus Neurons

(A) Schematic of experiments. The neurons in the dentate nucleus (DN, purple) and Purkinje cells (PCs) in the cerebellar cortex (lateral crus 1, green) were simultaneously recorded in mice performing the task.

(B) Injection of AAV expressing GFP in the cerebellar cortex marking the axons of PCs (green) projecting to the part of the DN (white outline) that was targeted for recordings. Coronal slice, counterstained with DAPI (blue).

(C–H) Examples of two recordings (first recording from C–E; second recording from F–H) in which PCs and DN neurons were simultaneously recorded.

(C and F) Running speed (RS, top) and lick rate (LR, bottom) are shown; mean (black line) ± SD (shaded area).

(D and G) PC spike raster plot (top) and mean firing rate of the same trials (bottom) are shown.

(E and H) Same as in (D) and (G) for simultaneously recorded DN neurons is shown.

(I) Cross-covariance between the activity of PCs and DN neurons from (D) and (E) (dark green) and (G) and (H) (light green) at different lags (5-ms bins).

(J and K) Average response profiles for all DN neurons (J) and all PCs (K) sorted by their mean firing rate (Z score) in the last second before reward. White vertical line indicates reward time.

(L) Distribution (bottom) and boxplot (median, 25th and 75th percentiles, and extremes, excluding outliers; top) of mean firing rate (Z score) in the last second before reward for PCs (green) and DN neurons (purple).

(M) Color-coded cross-correlograms (Z score) between all modulated PC-DN neuron pairs (n = 46/1,855 pairs; see STAR Methods).

(N) Average peristimulus histogram (Z score) ± SD for excited (orange, n = 6) and inhibited pairs (blue, n = 40). Note that the short latency inhibition is consistent with a monosynaptic inhibitory connection from PCs to DN neurons.

(O) Average shuffle-corrected cross-correlogram (Z score; see STAR Methods) for all putatively connected pairs showing a decrease in the probability of DN neuron firing in the seconds following PC activity. Trace is mean ± SD.

(P) Cross-correlogram (Z score) for an example PC-DN neuron pair. Grey shaded area indicates the time window for measuring the strength of connections (1–7 ms after PC spike; mean Z score value for this pair is indicated to the right of the shaded area).

(Q) Z score firing rate aligned to reward time (t = 0 s) for the PC (green) and DN neuron (purple) of the pair shown in (P). The correlation coefficient value for this pair is written on top of the traces.

(R) Strength of inhibition (measured as in P) versus correlation coefficient between the DN and PC peristimulus histograms in the 5 s before rewards (as in Q). Blue dots are from inhibited pairs, orange dots are excited pairs, and gray dots non-modulated pairs (see STAR Methods). Blue line and shaded area, linear fit of inhibited pairs with 95% confidence interval. Arrowhead indicates example pair shown in (P) and (Q).

Figure 4M). Six of these modulated pairs showed positive cross-correlations before the spike of the PC (Figures 4M and 4N). These are likely caused by common inputs exciting both the DN neuron and the PC. The other 40 pairs exhibited a millisecond-latency trough, consistent with monosynaptic inhibition from PC to DN neurons (Figures 4M and 4N). Over longer timescale, the average cross-correlogram between all putatively connected pairs revealed that PC inhibition onto DN neurons is fast, strong, and long lasting (Figure 4O; see STAR Methods). Thus, the ramping down of PC activity can relieve DN neurons of inhibition and allow extra-cerebellar inputs to drive their ramping activity in anticipation of reward (Figures 4P and 4Q). Finally, we found that the correlation between the response profiles of the putatively connected PC-DN neuron pairs was not linked to the strengths of their connection (i.e., PCs with positively correlated activity to that of DN neurons also substantially participated

to their inhibition; Figure 4R; p = 0.92; F test). Therefore, a learned decrease in the activity of ramping down PCs, rather than plasticity at the PC-DN neurons synapses, might explain the emergence of DN preparatory activity.

The best described form of plasticity in the cerebellar cortex is the long-term depression of parallel fiber to PC synapses under the control of teaching signals conveyed by climbing fibers (Raymond et al., 1996). To address whether PC activity in lateral crus 1 could be related to such a mechanism (Figure 5A), we first analyzed more closely the population of PCs exhibiting a decrease in activity before reward (n = 37/72, 4 mice; see STAR Methods). Activity of all PCs was modulated during running bouts and exhibited tuning to running speed (and/or visual flow speed) following linear or more complex relationships (Figure 5B). By fitting tuning curves of PC activity to running speed, we obtained linear model of firing rate for each PC
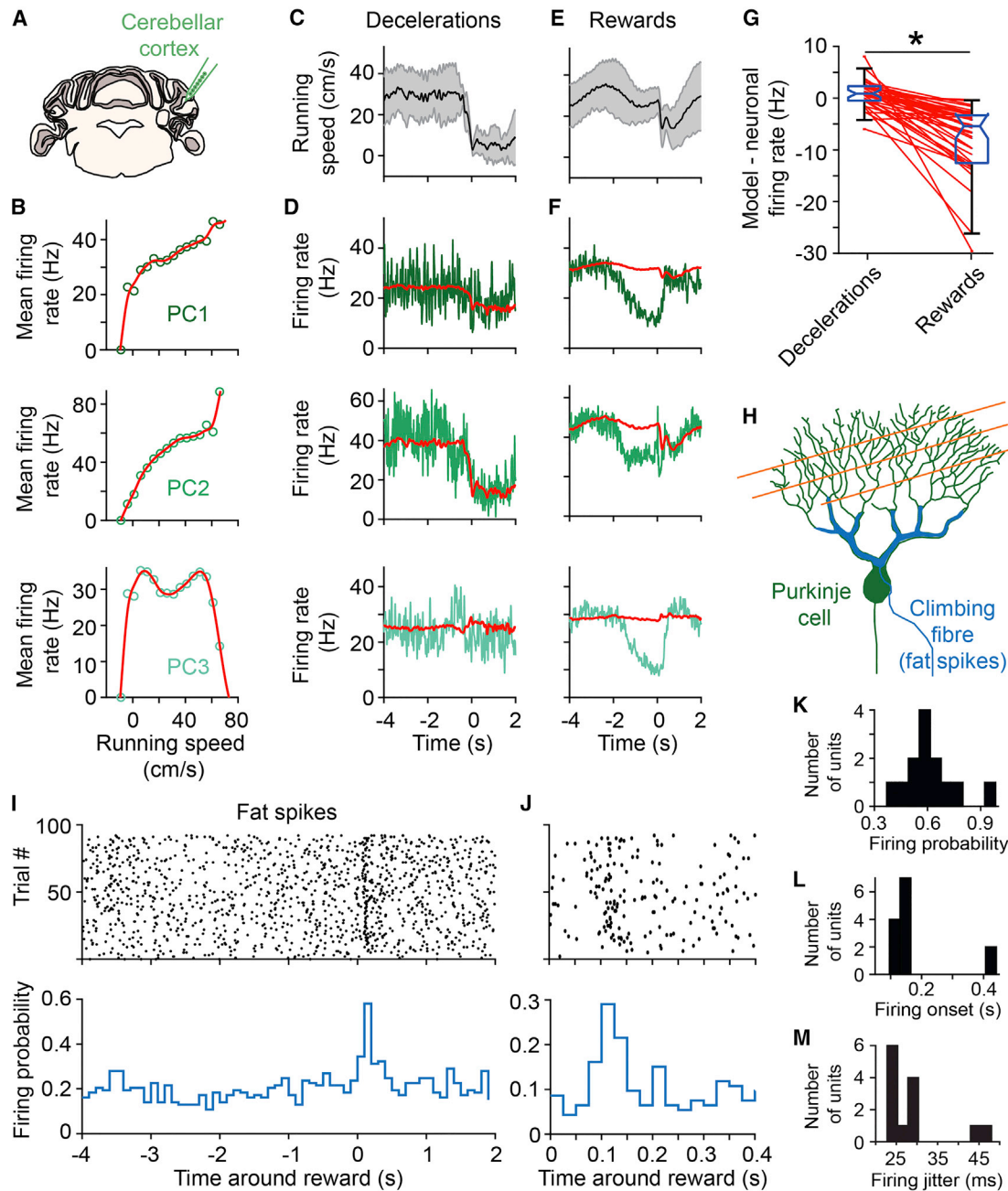
Figure 5. Evidence for Reward-Time-Based Supervised Learning in Lateral Crus 1 Purkinje Cells

(A) Schematic of experiments. Purkinje cell (PC) and climbing-fiber-related activity was recorded from lateral crus 1.

(B) Plot of firing rates as a function of running speed for 3 simultaneously recorded PCs. Green dots represent average firing rate for a given running speed bin (5 cm/s); the red line is the fit of the tuning curve obtained with a smoothing spline.

(C and D) Mean running speed (C, black line) and SD (gray shaded area) and mean firing rate of the 3 example PCs (D, green) and modeled firing rates obtained from the running speed tuning curves (red) shown in (B) around deceleration events outside of the reward zone (t = 0 s).

(E and F) Running speed (E) and firing profile of the same PCs (F) as in (D) centered on rewards (t = 0 s). Note the substantial deviation of firing rates from the model, specific to the reward context.

(G) Summary plot of mean remaining firing rate after subtracting the modeled activity for all PCs exhibiting decreased activity before reward (see STAR Methods), during the last 2 s before the events. Boxplots represent quartiles (non-outlier minimum, 25%, median, 75%, and non-outlier maximum values). Paired values from single neurons (red dots) in the decelerations (left column) and rewards (right column) conditions are linked by red lines. PC activity is significantly lower than that of the model in the reward context (star: p < 0.0005; Wilcoxon signed-rank test).

(legend continued on next page)

(see STAR Methods). The linear model captured well the mean PC firing rates during deceleration events outside of the reward zone (Figures 5C, 5D, and 5G). However, in comparison, the model significantly overestimated firing around rewards in most PCs (n = 25/37; Figures 5E–5G; see STAR Methods). This suggests that the strong decrease in the activity of most PCs prior to reward results from learned reductions in firing associated with the reward context. We thus looked for signatures of climbing fiber activity around reward times (Figure 5H). Climbing fiber discharges result in PC complex spikes (Figures S11D–S11F) that are also apparent as so-called fat spikes likely resulting from the large inward currents occurring in PC dendrites (Gao et al., 2012). We found that fat spikes were readily detectable in our recordings (Figures S11G and S11H), firing at characteristically low firing frequencies of climbing fiber discharges (Figure S11I; Zhou et al., 2014). Interestingly, 13/26 of the fat spikes units recorded in lateral crus 1 but 0/26 recorded in crus 2 exhibited a significant increase in their probability of firing (0.61 ± 0.15; Figures 5I–5K; see STAR Methods) shortly after reward delivery (177 ± 117 ms; Figures 5J and 5L), consistent with previous reports (Heffley et al., 2018; Ohmae and Medina, 2015). Moreover, the first fat spikes occurring after reward delivery exhibited relatively low jitter (29 ± 8 ms; Figures 5J and 5M), which may partly result from the variability in reward consumption across trials. Finally, plotting fat spike firing rates as a function of position inside the virtual corridor confirmed that they occurred most consistently shortly after rewards (Figures S11J and S11K). Thus, these putative climbing fiber events are well suited to report the timing of reward delivery to PCs and thereby shape the preceding decrease in their activity. Finally, we found that the reduction in PC firing occurred specifically in the reward context within the virtual corridor (Figures S3H and S3I). In summary, these data strongly suggest that lateral crus 1 PCs learn to predict the timing of upcoming rewards, shaping preparatory activity in the DN to provide a timed amplification signal to the neocortex.

Dynamics of Preparatory Activity across the Cerebello-Neocortical Circuit Are Consistent with Encoding Time between Cue and Reward Delivery

A likely role for preparatory activity is to anticipate the timing of future events based on past experience and environmental cues in order to produce accurately timed actions (Mauritz and Wise, 1986; Roux et al., 2003; Tsujimoto and Sawaguchi, 2005). If preparatory activity is related to predicting the timing of future rewards, the slope of preparatory activity may depend on the delay between the environmental cues and the reward; if this delay is long, preparatory activity should start early and progressively increase until reward delivery; and if the delay is short, preparatory activity should exhibit a steeper ramp. Moreover, the onset of preparatory activity should start at the appearance of the environmental cue, regardless of the delay to reward delivery. First, we used GLM classification to classify PCs to allow direct comparison with ALM and DN. Because, in our task, the delay between environmental cues and reward depends on mouse speed, we grouped trials according to mouse deceleration onset before rewards (Figure 6). The onset of preparatory activity in ALM (Figures 6A–6C), DN (Figures 6F–6H), and crus 1 cerebellar cortex (Figures 6K–6M) was closely related to the deceleration profiles, starting earlier in trials when mice decelerated sooner in anticipation of reward. Accordingly, in trials when mice decelerated closer to rewards, preparatory activity started later and exhibited a steeper ramp. The salient cue signifying the future occurrence of rewards is likely the onset of the second checkerboard corridor (Figure 1E). When plotting the same groups of trials around the appearance of the rewarded checkerboard, the onsets of deceleration and preparatory activity in type 1 and 2 neurons largely overlapped, starting around 1 s after the appearance of the rewarded checkboard, when mice have fully entered the reward zone (Figures 6D, 6E, 6I, 6J, 6N, and 6O). Because the firing of type 1 and 2 neurons in ALM and DN is not directly related to deceleration or licking (Figures 1 and 2), these data suggest that preparatory activity tracks the elapsed time from environmental cues predictive of reward.

DISCUSSION

Our results reveal a key contribution of the cerebellum in the generation of preparatory activity in the neocortex during goal-directed behavior. The DN—one of the output nuclei of the cerebellum—exhibits preparatory signals prior to reward acquisition that closely resemble those in the motor neocortex during motor preparation (Figures 1 and 2; see also Murakami et al., 2014; Rickert et al., 2009; Svoboda and Li, 2018). Silencing DN activity by photoactivation of PCs in lateral crus 1 caused a very short-latency decrease (<10 ms) in the activity of the majority of ALM neurons exhibiting preparatory activity (Figure 3). This result is consistent with observations that DN provides direct excitatory input to the motor thalamus (Ichinohe et al., 2000; Kelly and Strick, 2003; Middleton and Strick, 1997; Thach and Jones, 1979), which itself is essential for the generation of persistent activity in the neocortex (Guo et al., 2017; Reinhold et al., 2015). Our results also suggest that preparatory activity in the DN emerges via a transient, learned decrease in the activity of inhibitory PCs in lateral crus 1 during the period prior to reward acquisition (Figures 4 and 5). Thus, the cerebellum has a specific and fast driving influence on motor cortex activity in anticipation of actions required to acquire rewards. Our results agree with recent

---

(H) Schematic of a PC (green) and its two sources of inputs: parallel fibers (orange), which give rise to simple spikes, and the climbing fiber (blue), which gives rise to complex spikes also apparent as fat spikes (see Figure S11).

(I) Spike raster plot (top) and firing probability (100-ms binning, bottom) aligned on reward (t = 0 s) for an example fat spike unit.

(J) Same as (I) but focusing on the time period following reward with 25-ms binning.

(K) Distribution of firing probability for all fat spike units exhibiting significant increase in activity in the 500 ms after reward delivery (n = 13, 4 mice; see STAR Methods).

(L) Same as in (K) for firing onset (time of first spike in the first 100-ms bin of significant probability increase).

(M) Same as in (K) for firing jitter (mean difference between first spike times as in L).
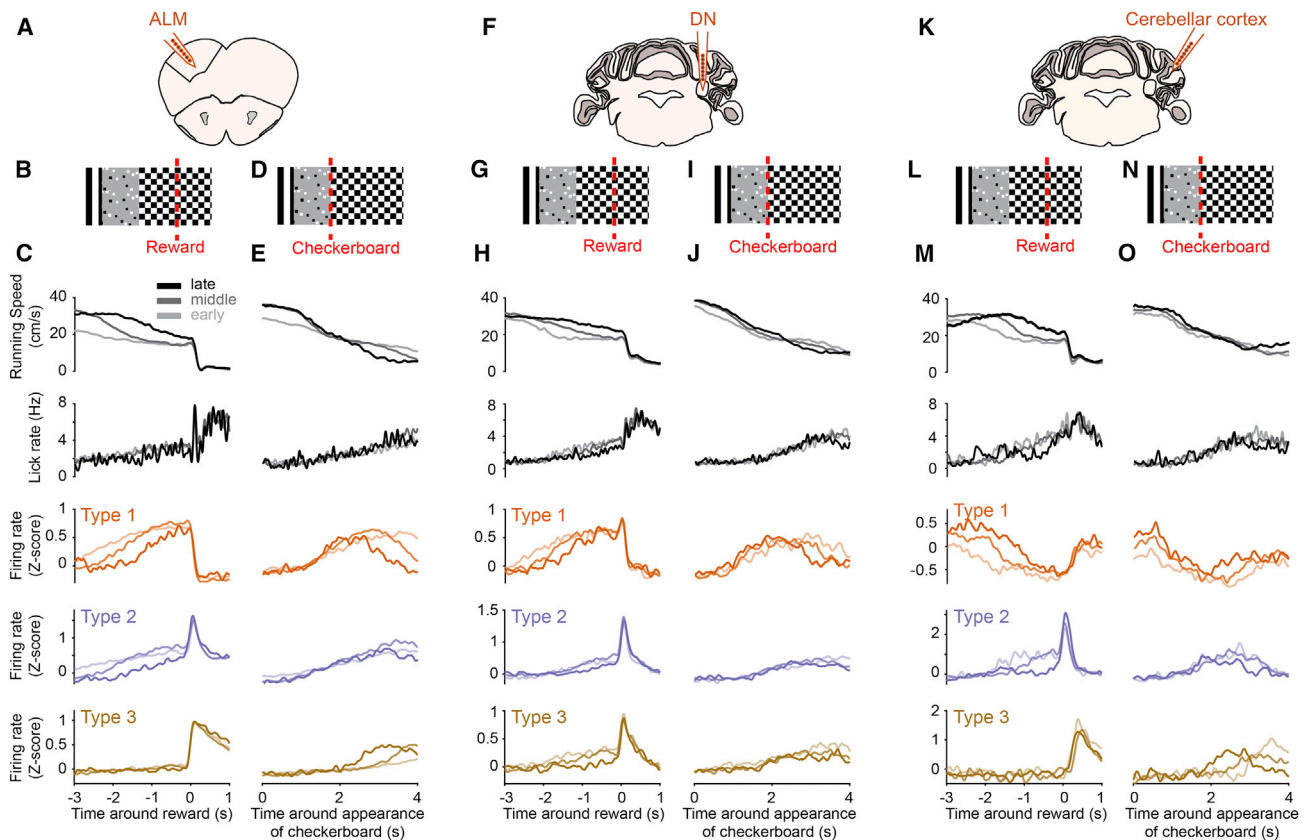
Figure 6. Dynamics of Preparatory Activity Suggest Reward Timing Prediction from Visual Cue

(A, F, and K) Schematic showing recording location in the anterolateral motor cortex (ALM, A), dentate nucleus (DN, F), and lateral crus 1 (K).

(B, G, and L) Schematic of virtual corridor showing the location of reward delivery (red dotted line).

(C, H, and M) From top to bottom, mean running speed, lick rate, and type 1–3 ALM (C), DN (H), or Purkinje cells (PCs) (M) firing rate (Z score) binned according to the time at which mouse speed dipped under 20 cm/s in the 4 s before reward (1st group: times below the 33rd percentile of the distribution; 2nd group: times between the 33rd and 66th percentile; 3rd group: times above the 66th).

(D, I, and N) Same as in (B), (G), and (L), with the red line denoting the appearance of the rewarded checkerboard.

(E, J, and O) Same as (C), (H), and (M) aligned to appearance of the rewarded checkerboard. Note the substantial decrease in onset jitter compared to reward-aligned traces (C), (H), and (M) for behavioral variables and type 1 or 2 neurons.

(M and O) PCs classified with GLM comprised 8 type 1 (all with decreasing activity), 4 type 2 (1 with decreasing and 3 with increasing activity), and 2 type 3 (all with increasing activity).

work on the role of deep cerebellar nuclei in shaping choice-related activity in ALM as mice perform a tactile discrimination task (Gao et al., 2018), and with human case studies that propose cerebellar contribution to a circuit involving motor thalamus and neocortex in the preparation of self-timed movements (Diener et al., 1989; Purzner et al., 2007).

The activity preceding goal-directed actions has been observed in many brain regions, but its significance is not well understood (Svoboda and Li, 2018). Our study suggests that the preparatory activity we observed in ALM and DN is not directly related to the execution of motor actions. First, although preparatory activity emerged before rewards along with mouse deceleration and anticipatory licks, we found no sign of such activity during deceleration or licking events outside of the reward zone (Figures 1N–1Q and 2J–2M). In fact, preparatory activity only emerged in the rewarded section of the virtual corridor (Figure S3). Those results are corroborated by the GLM classification

of neurons exhibiting preparatory activity, which found no significant relation between their spike times and lick times or running speed, even though other neurons modulated by licking and running speed were observed in ALM and DN populations (Figures 1F, 2B, and S2). Instead, our data argue that preparatory activity reflects a timing signal (Mauritz and Wise, 1986; Roux et al., 2003; Tsujimoto and Sawaguchi, 2005) that predicts the occurrence of the upcoming reward based on elapsed time from learned external cues (Figure 6), perhaps providing an "urgency" signal that amplifies or primes the emerging motor plan.

The cerebellum is known for its remarkable ability to learn the fine-scale temporal associations between internal and external context and specific actions (Kotani et al., 2003; Mauk and Buonomano, 2004; Medina, 2011; Perrett et al., 1993). We suggest that activity originating within motor-related and sensory areas of the neocortex is conveyed to the cerebellum via the cortico-pontine-mossy fiber pathway, where it may be combined with

reward prediction signals (Wagner et al., 2017) to adjust the timing of activity in preparation for goal-directed movements (Kunimatsu et al., 2018). The activity of PCs in lateral crus 1 was modulated by running and/or visual flow speed (Figures 5A–5D), consistent with this region receiving projections from the visual and hindlimb cortices (Figure S5). However, PC activity decreased significantly more prior to reward than predicted from mouse deceleration profiles (Figures 5B–5G). This additional activity decrease may result from long-term depression of parallel fiber inputs to PCs (Raymond et al., 1996) supervised by putative climbing fiber events that occur at reward delivery (Figures 5H–5M). Indeed, decreased activity in a large fraction of PCs in advance of reward acquisition is reminiscent of activity profiles resulting from associative learning in cerebellum-dependent tasks, such as eyelid conditioning (Freeman et al., 2005; Jirenhed et al., 2007), smooth pursuit (Medina and Lisberger, 2008), and saccadic eye movement tasks (Herzfeld et al., 2018). Additionally, reward time signaling from climbing fibers in lateral crus 1 is consistent with the view that the repertoire of climbing fiber activity extends beyond reporting motor errors and comprises signaling of salient events not directly related to motor performance (Heffley et al., 2018). We hypothesize that the cerebellum learns to predict upcoming rewards to sculpt the timing of preparatory signals generated in the neocortex and maintained in the thalamocortical loop.

The suppressive effects of cerebellar PC photoactivation on ALM activity were predominantly observed in neurons exhibiting preparatory activity prior to reward acquisition and much less in neurons that responded after reward delivery (Figures 3 and S7). The very short latency suppression suggests the involvement of the tri-synaptic pathway from cerebellar cortex to ALM neocortex (PC-DN-motor thalamus-ALM) is preferentially influencing a subset of ALM neurons that may be involved in motor planning (Svoboda and Li, 2018). Moreover, the short-latency nature of this effect discards the possibility that the disruption of preparatory activity results from the transient change in mouse motor behavior that followed PC photoactivation at longer delays.

Following cessation of PC photoactivation, the activity in ALM was rapidly reinstated. Because the contralateral ALM has been shown to reinstate preparatory activity at the end of the photoinhibition in the other hemisphere (Li et al., 2016), we examined whether bilateral PC photoactivation would prevent the recovery of ALM preparatory activity (Figure 3) and found that it did not (Figure S9). Although the cerebellar output contributes robustly to ALM activity (Figure 3), it is possible that other cortical regions involved in sensory processing or navigation keep track of the reward context and that this information re-establishes cerebello-cortical activity once this circuit recovers. The basal ganglia have also been shown to process preparatory activity (Kunimatsu et al., 2018; Ohmae et al., 2017) and might therefore contribute a separate subcortical signal for motor preparation.

Given that multiple closed-loop circuits have been identified between the subdivisions of cerebellum and the neocortex (Habas et al., 2009; Kelly and Strick, 2003; Middleton and Strick, 1997; Proville et al., 2014; Ramnani, 2006), we suggest that ALM and the lateral crus 1-DN cerebellar pathway constitutes one such circuit dedicated to the generation of precisely timed preparatory activity. A recent study has confirmed the existence of a full functional loop between ALM and the cerebellum, involving the DN and FN in maintaining choice-related signals (Gao et al., 2018). This study found that the disruption of DN activity impairs motor preparatory activity in ALM, in keeping with our results, but differences in the effect of manipulating DN and FN activity on ALM choice signals (Gao et al., 2018). Further work will be required to dissect the cerebellar computation giving rise to the FN output involved in motor preparation and how it may complement the role of the lateral crus 1-DN circuit.

More generally, our data add to the growing body of evidence that persistent activity in the neocortex is not a result of recurrent neural interactions within local circuits but instead requires the coordination of activity across distal brain regions (Gao et al., 2018; Guo et al., 2017; Reinhold et al., 2015; Schmitt et al., 2017; Siegel and Mauk, 2013). The fact that neurons in the deep cerebellar nuclei send excitatory projections to other thalamic regions subserving non-motor cortical areas (Kelly and Strick, 2003; Middleton and Strick, 1997) suggests that they may contribute to the maintenance of persistent neocortical activity during cognitive tasks requiring attention and working memory (Baumann et al., 2015; Gao et al., 2018; Siegel and Mauk, 2013; Sokolov et al., 2017; Strick et al., 2009).

STAR★METHODS

Detailed methods are provided in the online version of this paper and include the following:

- KEY RESOURCES TABLE
- CONTACT FOR REAGENT AND RESOURCE SHARING
- EXPERIMENTAL MODEL AND SUBJECT DETAILS
- METHOD DETAILS
  - Animal care and housing
  - Behavior
  - Virus and tracer injection
  - Intrinsic signal imaging
  - *In vivo* extracellular electrophysiology
  - Photoactivation
- QUANTIFICATION AND STATISTICAL ANALYSIS
  - Electrophysiology data analysis
  - Classification of cerebellar cortex and ALM units
  - Generalized linear model
  - Linear modeling of Purkinje cells firing rate from running speed

SUPPLEMENTAL INFORMATION

Supplemental Information can be found online at https://doi.org/10.1016/j.neuron.2019.05.022.

CellPress

AUTHOR CONTRIBUTIONS

DECLARATION OF INTERESTS

REFERENCES

Angaut, P., and Bowsher, D. (1970). Ascending projections of the medial cerebellar (fastigial) nucleus: an experimental study in the cat. Brain Res. 24, 49–68.

Ashmore, R.C., and Sommer, M.A. (2013). Delay activity of saccade-related neurons in the caudal dentate nucleus of the macaque cerebellum. J. Neurophysiol. 109, 2129–2144.

Baumann, O., Borra, R.J., Bower, J.M., Cullen, K.E., Habas, C., Ivry, R.B., Leggio, M., Mattingley, J.B., Molinari, M., Moulton, E.A., et al. (2015). Consensus paper: the role of the cerebellum in perceptual processes. Cerebellum 14, 197–220.

Blot, A., de Solages, C., Ostojic, S., Szapiro, G., Hakim, V., and Léna, C. (2016). Time-invariant feed-forward inhibition of Purkinje cells in the cerebellar cortex in vivo. J. Physiol. 594, 2729–2749.

Churchland, M.M., Santhanam, G., and Shenoy, K.V. (2006). Preparatory activity in premotor and motor cortex reflects the speed of the upcoming reach. J. Neurophysiol. 96, 3130–3146.

de Solages, C., Szapiro, G., Brunel, N., Hakim, V., Isope, P., Buisseret, P., Rousseau, C., Barbour, B., and Léna, C. (2008). High-frequency organization and synchrony of activity in the Purkinje cell layer of the cerebellum. Neuron 58, 775–788.

Diener, H.C., Dichgans, J., Guschlbauer, B., Bacher, M., and Langenbach, P. (1989). Disturbances of motor preparation in basal ganglia and cerebellar disorders. Prog. Brain Res. 80, 481–488, discussion 479–480.

Freeman, J.H.J., Jr., Halverson, H.E., and Poremba, A. (2005). Differential effects of cerebellar inactivation on eyeblink conditioned excitation and inhibition. J. Neurosci. 25, 889–895.

Funahashi, S., Bruce, C.J., and Goldman-Rakic, P.S. (1989). Mnemonic coding of visual space in the monkey's dorsolateral prefrontal cortex. J. Neurophysiol. 61, 331–349.

Fuster, J.M., and Alexander, G.E. (1971). Neuron activity related to short-term memory. Science 173, 652–654.

Gao, H., Solages, Cd., and Lena, C. (2012). Tetrode recordings in the cerebellar cortex. J. Physiol. Paris 106, 128–136.

Gao, Z., Davis, C., Thomas, A.M., Economo, M.N., Abrego, A.M., Svoboda, K., De Zeeuw, C.I., and Li, N. (2018). A cortico-cerebellar loop for motor planning. Nature 563, 113–116.

Giovannucci, A., Badura, A., Deverett, B., Najafi, F., Pereira, T.D., Gao, Z., Ozden, I., Kloth, A.D., Pnevmatikakis, E., Paninski, L., et al. (2017). Cerebellar granule cells acquire a widespread predictive feedback signal during motor learning. Nat. Neurosci. 20, 727–734.

Guo, Z.V., Li, N., Huber, D., Ophir, E., Gutnisky, D., Ting, J.T., Feng, G., and Svoboda, K. (2014). Flow of cortical activity underlying a tactile decision in mice. Neuron 81, 179–194.

Guo, Z.V., Inagaki, H.K., Daie, K., Druckmann, S., Gerfen, C.R., and Svoboda, K. (2017). Maintenance of persistent activity in a frontal thalamocortical loop. Nature 545, 181–186.

Habas, C., Kamdar, N., Nguyen, D., Prater, K., Beckmann, C.F., Menon, V., and Greicius, M.D. (2009). Distinct cerebellar contributions to intrinsic connectivity networks. J. Neurosci. 29, 8586–8594.

Heffley, W., Song, E.Y., Xu, Z., Taylor, B.N., Hughes, M.A., McKinney, A., Joshua, M., and Hull, C. (2018). Coordinated cerebellar climbing fiber activity signals learned sensorimotor predictions. Nat. Neurosci. 21, 1431–1441.

Herzfeld, D.J., Kojima, Y., Soetedjo, R., and Shadmehr, R. (2018). Encoding of error and learning to correct that error by the Purkinje cells of the cerebellum. Nat. Neurosci. 21, 736–743.

Hoover, W.B., and Vertes, R.P. (2007). Anatomical analysis of afferent projections to the medial prefrontal cortex in the rat. Brain Struct. Funct. 212, 149–179.

Huang, C.C., Sugino, K., Shima, Y., Guo, C., Bai, S., Mensh, B.D., Nelson, S.B., and Hantman, A.W. (2013). Convergence of pontine and proprioceptive streams onto multimodal cerebellar granule cells. eLife 2, e00400.

Ichinohe, N., Mori, F., and Shoumura, K. (2000). A di-synaptic projection from the lateral cerebellar nucleus to the laterodorsal part of the striatum via the central lateral nucleus of the thalamus in the rat. Brain Res. 880, 191–197.

Jirenhed, D.-A., Bengtsson, F., and Hesslow, G. (2007). Acquisition, extinction, and reacquisition of a cerebellar cortical memory trace. J. Neurosci. 27, 2493–2502.

Jörntell, H., and Ekerot, C.F. (1999). Topographical organization of projections to cat motor cortex from nucleus interpositus anterior and forelimb skin. J. Physiol. 514, 551–566.

Kelly, R.M., and Strick, P.L. (2003). Cerebellar loops with motor cortex and prefrontal cortex of a nonhuman primate. J. Neurosci. 23, 8432–8444.

Kennedy, A., Wayne, G., Kaifosh, P., Alviña, K., Abbott, L.F., and Sawtell, N.B. (2014). A temporal basis for predicting the sensory consequences of motor commands in an electric fish. Nat. Neurosci. 17, 416–422.

Khilkevich, A., Canton-Josh, J., DeLord, E., and Mauk, M.D. (2018). A cerebellar adaptation to uncertain inputs. Sci. Adv. 4, p9660.

Kopec, C.D., Erlich, J.C., Brunton, B.W., Deisseroth, K., and Brody, C.D. (2015). Cortical and subcortical contributions to short-term memory for orienting movements. Neuron 88, 367–377.

Kotani, S., Kawahara, S., and Kirino, Y. (2003). Purkinje cell activity during learning a new timing in classical eyeblink conditioning. Brain Res. 994, 193–202.

Kubota, K., and Hamada, I. (1979). Preparatory activity of monkey pyramidal tract neurons related to quick movement onset during visual tracking performance. Brain Res. 168, 435–439.

Kunimatsu, J., Suzuki, T.W., Ohmae, S., and Tanaka, M. (2018). Different contributions of preparatory activity in the basal ganglia and cerebellum for self-timing. eLife 7, e35676.

Leergaard, T.B., Lillehaug, S., De Schutter, E., Bower, J.M., and Bjaalie, J.G. (2006). Topographical organization of pathways from somatosensory cortex through the pontine nuclei to tactile regions of the rat cerebellar hemispheres. Eur. J. Neurosci. 24, 2801–2812.

Li, N., Chen, T.-W., Guo, Z.V., Gerfen, C.R., and Svoboda, K. (2015). A motor cortex circuit for motor planning and movement. Nature 519, 51–56.

Li, N., Daie, K., Svoboda, K., and Druckmann, S. (2016). Robust neuronal dynamics in premotor cortex during motor planning. Nature 532, 459–464.

Raymond, J.L., Lisberger, S.G., and Mauk, M.D. (1996). The cerebellum: a neuronal learning machine? Science 272, 1126–1131.

Lu, X., Miyachi, S., Ito, Y., Nambu, A., and Takada, M. (2007). Topographic distribution of output neurons in cerebellar nuclei and cortex to somatotopic map of primary motor cortex. Eur. J. Neurosci. 25, 2374–2382.

Mauk, M.D., and Buonomano, D.V. (2004). The neural basis of temporal processing. Annu. Rev. Neurosci. 27, 307–340.

Mauritz, K.H., and Wise, S.P. (1986). Premotor cortex of the rhesus monkey: neuronal activity in anticipation of predictable environmental events. Exp. Brain Res. 61, 229–244.

McCrea, R.A., Bishop, G.A., and Kitai, S.T. (1978). Morphological and electrophysiological characteristics of projection neurons in the nucleus interpositus of the cat cerebellum. J. Comp. Neurol. 181, 397–419.

Medina, J.F. (2011). The multiple roles of Purkinje cells in sensori-motor calibration: to predict, teach and command. Curr. Opin. Neurobiol. *21*, 616–622.

Medina, J.F., and Lisberger, S.G. (2008). Links from complex spikes to local plasticity and motor learning in the cerebellum of awake-behaving monkeys. Nat. Neurosci. *11*, 1185–1192.

Middleton, F.A., and Strick, P.L. (1997). Cerebellar output channels. Int. Rev. Neurobiol. *41*, 61–82.

Murakami, M., Vicente, M.I., Costa, G.M., and Mainen, Z.F. (2014). Neural antecedents of self-initiated actions in secondary motor cortex. Nat. Neurosci. *17*, 1574–1582.

Ohmae, S., and Medina, J.F. (2015). Climbing fibers encode a temporal-difference prediction error during cerebellar learning in mice. Nat. Neurosci. *18*, 1798–1803.

Ohmae, S., Kunimatsu, J., and Tanaka, M. (2017). Cerebellar roles in self-timing for sub- and supra-second intervals. J. Neurosci. *37*, 3511–3522.

Pachitariu, M., Steinmetz, N., Kadir, S., Carandini, M., and Harris, K.D. (2016). Kilosort: realtime spike-sorting for extracellular electrophysiology with hundreds of channels. bioRxiv. https://doi.org/10.1101/061481.

Park, I.M., Meister, M.L.R., Huk, A.C., and Pillow, J.W. (2014). Encoding and decoding in parietal cortex during sensorimotor decision-making. Nat. Neurosci. *17*, 1395–1403.

Payne, J.N. (1983). The cerebellar nucleo-cortical projection in the rat studied by the retrograde fluorescent double-labelling method. Brain Res. *271*, 141–144.

Paz, R., Boraud, T., Natan, C., Bergman, H., and Vaadia, E. (2003). Preparatory activity in motor cortex reflects learning of local visuomotor skills. Nat. Neurosci. *6*, 882–890.

Perrett, S.P., Ruiz, B.P., and Mauk, M.D. (1993). Cerebellar cortex lesions disrupt learning-dependent timing of conditioned eyelid responses. J. Neurosci. *13*, 1708–1718.

Person, A.L., and Raman, I.M. (2011). Purkinje neuron synchrony elicits time-locked spiking in the cerebellar nuclei. Nature *481*, 502–505.

Proville, R.D., Spolidoro, M., Guyon, N., Dugué, G.P., Selimi, F., Isope, P., Popa, D., and Léna, C. (2014). Cerebellum involvement in cortical sensorimotor circuits for the control of voluntary movements. Nat. Neurosci. *17*, 1233–1239.

Purzner, J., Paradiso, G.O., Cunic, D., Saint-Cyr, J.A., Hoque, T., Lozano, A.M., Lang, A.E., Moro, E., Hodaie, M., Mazzella, F., and Chen, R. (2007). Involvement of the basal ganglia and cerebellar motor pathways in the preparation of self-initiated and externally triggered movements in humans. J. Neurosci. *27*, 6029–6036.

Ramnani, N. (2006). The primate cortico-cerebellar system: anatomy and function. Nat. Rev. Neurosci. *7*, 511–522.

Reinhold, K., Lien, A.D., and Scanziani, M. (2015). Distinct recurrent versus afferent dynamics in cortical visual processing. Nat. Neurosci. *18*, 1789–1797.

Rickert, J., Riehle, A., Aertsen, A., Rotter, S., and Nawrot, M.P. (2009). Dynamic encoding of movement direction in motor cortical neurons. J. Neurosci. *29*, 13870–13882.

Roux, S., Coulmance, M., and Riehle, A. (2003). Context-related representation of timing processes in monkey motor cortex. Eur. J. Neurosci. *18*, 1011–1016.

Saunders, A., Johnson, C.A., and Sabatini, B.L. (2012). Novel recombinant adeno-associated viruses for Cre activated and inactivated transgene expression in neurons. Front. Neural Circuits *6*, 47.

Sawyer, S.F., Tepper, J.M., and Groves, P.M. (1994). Cerebellar-responsive neurons in the thalamic ventroanterior-ventrolateral complex of rats: light and electron microscopy. Neuroscience *63*, 725–745.

Schmitt, L.I., Wimmer, R.D., Nakajima, M., Happ, M., Mofakham, S., and Halassa, M.M. (2017). Thalamic amplification of cortical connectivity sustains attentional control. Nature *545*, 219–223.

Shakkottai, V.G. (2014). Physiologic changes associated with cerebellar dystonia. Cerebellum *13*, 637–644.

Shinoda, Y., Kano, M., and Futami, T. (1985). Synaptic organization of the cerebello-thalamo-cerebral pathway in the cat. I. Projection of individual cerebellar nuclei to single pyramidal tract neurons in areas 4 and 6. Neurosci. Res. *2*, 133–156.

Siegel, J.J., and Mauk, M.D. (2013). Persistent activity in prefrontal cortex during trace eyelid conditioning: dissociating responses that reflect cerebellar output from those that do not. J. Neurosci. *33*, 15272–15284.

Siegle, J.H., López, A.C., Patel, Y.A., Abramov, K., Ohayon, S., and Voigts, J. (2017). Open Ephys: an open-source, plugin-based platform for multichannel electrophysiology. J. Neural Eng. *14*, 045003.

Sokolov, A.A., Miall, R.C., and Ivry, R.B. (2017). The cerebellum: adaptive prediction for movement and cognition. Trends Cogn. Sci. *21*, 313–332.

Strick, P.L., Dum, R.P., and Fiez, J.A. (2009). Cerebellum and nonmotor function. Annu. Rev. Neurosci. *32*, 413–434.

Suzuki, L., Coulon, P., Sabel-Goedknegt, E.H., and Ruigrok, T.J.H. (2012). Organization of cerebral projections to identified cerebellar zones in the posterior cerebellum of the rat. J. Neurosci. *32*, 10854–10869.

Svoboda, K., and Li, N. (2018). Neural mechanisms of movement planning: motor cortex and beyond. Curr. Opin. Neurobiol. *49*, 33–41.

Tanaka, M. (2007). Cognitive signals in the primate motor thalamus predict saccade timing. J. Neurosci. *27*, 12109–12118.

Tanji, J., and Evarts, E.V. (1976). Anticipatory activity of motor cortex neurons in relation to direction of an intended movement. J. Neurophysiol. *39*, 1062–1068.

Thach, W.T., and Jones, E.G. (1979). The cerebellar dentatothalamic connection: terminal field, lamellae, rods and somatotopy. Brain Res. *169*, 168–172.

Tsujimoto, S., and Sawaguchi, T. (2005). Neuronal activity representing temporal prediction of reward in the primate prefrontal cortex. J. Neurophysiol. *93*, 3687–3692.

Voogd, J. (2014). What we do not know about cerebellar systems neuroscience. Front. Syst. Neurosci. *8*, 227.

Wagner, M.J., Kim, T.H., Savall, J., Schnitzer, M.J., and Luo, L. (2017). Cerebellar granule cells encode the expectation of reward. Nature *544*, 96–100.

Wise, S.P. (1985). The primate premotor cortex: past, present, and preparatory. Annu. Rev. Neurosci. *8*, 1–19.

Zhou, H., Lin, Z., Voges, K., Ju, C., Gao, Z., Bosman, L.W.J., Ruigrok, T.J., Hoebeek, F.E., De Zeeuw, C.I., and Schonewille, M. (2014). Cerebellar modules operate at different frequencies. eLife *3*, e02536.

STAR★METHODS

KEY RESOURCES TABLE

REAGENT or RESOURCE	SOURCE	IDENTIFIER
Bacterial and Virus Strains		
pAAV-Ef1a-DO-EGFP-WPRE-pA	Saunders et al., 2012	RRID: Addgene_37085
Experimental Models: Organisms/Strains		
Mouse: C57BL/6JRj	Janvier Labs	N/A
Mouse: B6.129-Tg(Pcp2-cre)2Mpin/J	The Jackson Laboratory	JAX: 004146
Mouse: B6;129S-Gt(ROSA)26Sortm32(CAG-COP4*H134R/EYFP)Hze/J	The Jackson Laboratory	JAX: 012569
Software and Algorithms		
MATLAB	MathWorks; https://www.mathworks.com	RRID: SCR_00162
Open Ephys	http://www.open-ephys.org	N/A
neuroGLM	https://github.com/pillowlab/neuroGLM	N/A

CONTACT FOR REAGENT AND RESOURCE SHARING

Further information and requests for resources and reagents should be directed to and will be fulfilled by the Lead Contact, Thomas D. Mrsic-Flogel (t.mrsic-flogel@ucl.ac.uk).

EXPERIMENTAL MODEL AND SUBJECT DETAILS

All experimental procedures were carried out in accordance with institutional animal welfare guidelines and licensed by the Veterinary Office of the Canton of Basel, Switzerland or under the UK Animals (Scientific Procedures) Act of 1986 (PPL 70/8116) following local ethical approval. For this study we used 35 male C57BL6 mice (supplied by Janvier labs) and 10 mice (7 males, 3 females) from a transgenic cross between B6;129S-Gt(ROSA)26Sortm32(CAG-COP4*H134R/EYFP)Hze/J and B6.129-Tg(Pcp2-cre)2Mpin/J lines (The Jackson Laboratory) aged > 60 days postnatal.

METHOD DETAILS

Animal care and housing

Animals were housed in a reverse 12:12 h light/dark cycle and were food-restricted starting a week after surgery with maximum 20% weight loss. Surgical procedures were carried out aseptically on animals subcutaneously injected with atropine (0.1 mg kg^{-1}), dexamethasone (2mg kg^{-1}), and a general anesthetic mixed comprising fentanyl (0.05 mg kg^{-1}), midazolam (5mg kg^{-1}), and medetomidine (0.5mg kg^{-1}). Animals were injected an analgesic (buprenorphine, 0.1 mg kg^{-1}), and antibiotics (enrofloxacin, 5 mg kg^{-1}) at least 15 min prior to the end of the surgery and once every day for two days post-surgery. For intrinsic imaging mice were under 1%–2% isoflurane anesthesia. For acute electrophysiological recordings mice were put under 1%–2% isoflurane anesthesia during the craniotomy procedure and allowed to recover for 1-2 h before recording.

Behavior

Mice were trained for 1-2 weeks to run head-fixed on a Styrofoam cylinder in front of two computer monitors placed 22 cm away from their eyes. Mice were trained only once per day with training duration being 15 min on the first day, 30 min on the second and third days, and 1 h per day from then-on regardless of the number of trials performed. Running speed was calculated from the tick count of an optical rotary encoder placed on the axis of the wheel with a Teensy USB development board and was fed back as position to a Unity software to display visual flow of a virtual corridor using a MATLAB-based script. A reward delivery spout was positioned under the snout of the mouse from which a drop of soy milk was delivered at a defined position inside the corridor (at 360 cm from start). Licks were detected with a piezo disc sensor placed under the spout and signals were sent to the Teensy USB development board and extracted as digital signals. The virtual corridor was composed of a black and white random dot pattern on a gray background (80 cm long) followed by black and white checkerboard (40 cm long), black and white random triangle pattern on a gray background (80 cm long), vertical black and white grating (40 cm long), black and white random square pattern on a gray background (80 cm long), and a final black and white checkerboard inside which reward was delivered 40 cm from its beginning. The checkerboard pattern was

maintained for 2.5 s following reward delivery, after which the corridor was reset to the starting position. Mice were initially trained on a short version of the corridor (20, 10, 20, 10, 20 cm length for each visual pattern respectively, and reward position at 90 cm), before extending the corridor to full length. Appearance of the visual patterns inside the virtual corridor was signaled by TCP when the mouse reached the corresponding position in the virtual corridor. In 4/5 mice shown in Figure 3, 3/3 mice from Figure S9 and 3/3 mice from Figure S10, the corridor started at 120 cm distance from start to increase the number of trials.

Virus and tracer injection

AAV2/1-Ef1a-eGFP-WPRE (30nl, 1.5e^{11} titer) was injected over 15-30 min with a *Toohey* Spritzer *Pressure System* (*Toohey Company*) with pulse duration from 5 to 20 ms delivered at 1Hz with pressure between 5 and 15 psi into the left cerebellar crus 1 at the following coordinates: 6 mm posterior to Bregma, 3.3 mm mediolateral, and at a depth of 200 μm. Two weeks after injection mice were euthanized with a dose of pentobarbital (80 mg kg^{-1}) and transcardially perfused with 4% paraformaldehyde. Perfused brains were put inside a block of agarose and sliced at 100 μm with a microtome. Slices were then mounted with a mixture of mounting medium and DAPI staining and imaged on a Zeiss LSM700 confocal microscope with a 40X oil objective.

Intrinsic signal imaging

Mice were anesthetized under 1%–2% isoflurane and placed in a stereotaxic frame. A scalp incision was made along the midline of the head and the skull was cleaned and scraped. Two 80 μm tungsten wires (GoodFellow) were inserted inside polyimide tubes (230 μm O.D., 125 μm I.D.) and implanted 300 μm apart into the right primary visual (VisP) and limb motor cortex (lM1) following stereotaxic coordinates (2.7 posterior and 2.5 mm lateral to bregma, 0.25 anterior and 1.5 mm lateral to bregma, respectively) at 800 μm depth from the surface of the brain. Dental cement was added to join the wires to the skull. Neck muscles covering the bone over the cerebellum on the left side were gently detached and cut with fine scissors. The surface of the cerebellum was then carefully cleaned.

Animals were then placed inside a custom-built frame to incline the head and expose the surface of the bone above the cerebellum for imaging with a tandem lens macroscope. Mineral oil was applied to allow imaging through the bone. The mouse was lightly anaesthetized with 0.5%–1% isoflurane and the body temperature monitored with a rectal probe and maintained at 37°C. The preparation was illuminated with 700 nm light from an LED source and the imaging plane was focused 300 μm below the skull surface. Images were acquired through a bandpass filter centered at 700 nm with 10 nm bandwidth (Edmund Optics) at 6.25 Hz with a 12-bit CCD camera (1300QF; VDS Vossküller) connected to a frame grabber (PCI-1422; National Instruments).

Tungsten wires were clamped with micro alligator clips and connected to a stimulus isolator (A395; World Precision Instruments). After a 10 s long baseline, trains of 700 μA stimuli were delivered at 6 Hz with pulse duration of 200 μs for 3 s to each cortical area alternatively, followed by a 10 s long recovery phase. Averages of 20 trials were calculated and hemodynamic signals were measured relative to the last 3 s before stimulation ($\Delta F/F_0$). Location of tungsten electrodes inside the neocortex were confirmed post hoc with DiI labeling of the tracts.

In vivo extracellular electrophysiology

Mice were anaesthetized according to the surgical procedure described in the animal care and housing section and placed into a stereotaxic frame. The skin over the skull was incised along the midline and the skull was cleaned and scrapped. A headplate was then attached to the skull in front of the cerebellum using Super Bond dental cement (Super-Bond C&B). For cerebellar recordings the neck muscles covering the bone were gently detached and cut with fine scissors on the left side. The surface of the skull over the cerebellum was then cleaned, a small piece of curved plastic was glued to the base of the exposed skull to support a well attached to the headplate and built up with dental cement and Tetric EvoFlow (Ivoclar Vivadent). The well was then filled with Kwik-Cast sealant (World Precision Instruments). For the simultaneous recordings in cerebellum and ALM, a small additional well was built around stereotaxically-defined coordinates for the right ALM (2.5 mm anterior and 1.5 mm lateral to bregma).

On the day of the recording mice were anaesthetized under 1%–2% isoflurane and small craniotomies (1mm diameter) were made above left lateral crus 1 (6 mm posterior and 3.3 mm lateral to bregma), left dentate nucleus (6 mm posterior, and 2.25 mm lateral to bregma) and/or right ALM (2.5 mm anterior and 1.5 mm lateral to bregma). Mice recovered from surgery for 1-2 h before recording. Mice were then head-fixed over a Styrofoam cylinder. The well(s) around the craniotomy(ies) were filled with cortex buffer containing (in mM) 125 NaCl, 5 KCl, 10 Glucose monohydrate, 10 HEPES, 2 MgSO$_4$ heptahydrate, 2 CaCl$_2$ adjusted to pH 7.4 with NaOH. A silver wire was placed in the bath for referencing. Extracellular spikes were recorded using NeuroNexus silicon probes (A2x32-5mm-25-200-177-A64). The 64- or 128-channel voltages were acquired through amplifier boards (RHD2132, Intant Technologies) at 30 kHz per channel, serially digitized and send to an Open Ephys acquisition board via a SPI interface cable (Siegle et al., 2017). Mice were recorded up to 90 min only once regardless of the number of trials performed (ranges from 36 to 333, 137 ± 86 mean and SD) except for 1/5 mouse from Figure 3 and 2/6 mice from Figures S9 and S10 that were recorded over 2 consecutive days, in which case the cement wells around the craniotomies were filled with Kwik-Sil (World Precision Instruments) and sealed with Tetric EvoFlow after the first recording session.

Photoactivation

A 200 μm diameter optical fiber was placed on top of the surface of left lateral crus 1 using a manual micromanipulator. Light was delivered by a 100 mW 473 nm laser (CNI, MBL-III-473) triggered by a Pulse Pal pulse train generator (Open Ephys) using 1 s

long square pulses (n = 5 recordings, 5 mice). In one additional recording (data included in Figures 3L–3Q) the photoactivation period lasted 2 s. To prevent mice from seeing the laser light, a masking 470 nm light from a fiber-coupled LED (Thorlabs) was placed in front of the connector between the patch cable and the optical fiber and turned on during the whole recording session. Mice were also trained in the presence of LED light. Black varnish was painted over the cement well surrounding the craniotomy and black tape was wrapped around the connection between the patch cable and the optical fiber. One-second square light pulses (5 to 10 mW) were randomly delivered in 40% of trials (at least 10 trials, n = 38 ± 28, mean and SD from 5 mice). Control trials from mice that experienced photoactivation were not included in Figures 1 and 2 to avoid confounding effects such as plasticity-induced change in neuronal activity. For bilateral crus 1 photoactivation, a second 200 μm diameter optical fiber was placed over the right crus 1 and was coupled to a second 80 mW Stradus 473-80 nm laser (Vortran Laser Technology, Inc). The light pulses were set as square onsets, continuous voltage for 700 ms (1 to 4.5 mW), and ramp offsets in the last 300 ms to limit the rebound of activity in DCN neurons. Unilateral (left lateral crus 1 only) and bilateral stimulations occurred randomly in 40% of trials (at least 10 trials each, n = 24 ± 17 and 24 ± 16, mean and SD from 3 mice). The same protocol was used for lateral crus 1 versus lobule IV-V photoactivation (n = 26 ± 10 and 33 ± 32 trials, mean and SD from 3 mice).

QUANTIFICATION AND STATISTICAL ANALYSIS

Electrophysiology data analysis

Spikes were sorted with Kilosort (https://github.com/cortex-lab/Kilosort) using procedures previously described (Pachitariu et al., 2016). Briefly, the extracellular voltage recordings were high-pass filtered at 300 Hz, the effect of recording artifacts and correlated noise across channels were reduced using common average referencing and data whitening. Putative spikes were detected using an amplitude threshold (4 SD of baseline) over the filtered voltage trace and matched to template waveforms. The firing rate for each unit was estimated by convolving a Gaussian kernel with spike times; σ was chosen according to the median inter-spike interval of each individual unit. For population scatterplots and averaging across neuronal activities grouped by type we used the Z-score of firing rates.

The cross-correlogram between each PC and DN neuron simultaneously recorded (n = 1855 pairs, 3 mice) was computed with a bin of 1 ms (Figure 4M). A correlogram was considered as modulated if at least two consecutive bins in the 10 ms following the Purkinje cell spike were above 3 SD of the baseline computed in the [-50, −10] window. For all these pairs (46/1855) the cross-correlogram was Z-scored by the mean/SD of this baseline and all Z-scored correlograms were averaged. The strength of connection was measured as the average of the Z-scored correlograms between 1 and 7 ms (Figure 4P) and pairs were split between excited (n = 6) and inhibited (n = 40) based on the sign of this average. For Figure 4Q, the response profiles of PCs and DN neurons around reward time were computed and Z-scored using a baseline taken between −10 and −5 s. For inhibited pairs, the spearman correlation coefficient of these response profiles in the 5 s before reward was correlated to the strength of connection using a linear regression model (MATLAB fitlm, blue line Figure 4R). Shaded area indicates the 95% confidence intervals.

On longer timescale, task modulation of the neurons entrains instabilities of the firing rate that might produce spurious covariance between comodulated pairs. To assess the relation between PC activity and DN neuron activity on these timescales we used two equivalent methods. In Figure 4I, the cross-covariance between firing rates of PC and DN pairs was corrected for correlated firing resulting from stimulus effects by subtracting the cross-covariance between shuffled trials and was then normalized by the variance of the firing rates. In Figure 4O, the cross-correlogram between each pair was first calculated on each trial in the last 10 s before the reward (CC_{raw}). We then computed the cross-correlogram for the same pair but using trial n and n+1 ($CC_{shuffled}$). The shuffled corrected correlogram was then defined as ($CC_{raw} − CC_{shuffled}$) / sqrt($CC_{shuffled}$) and averaged across pairs.

ALM neurons were considered modulated by cerebellar photoactivation if the average firing rate in the second following the onset of photostimulation was significantly (rank-sum, alpha of 0.05) different from the average firing rate during the same window in control trials. We classified them as excited/inhibited if the control response was lower/higher than that during photoactivation trials. Average firing rate of the population in the same 1 s window were compared between control and photoactivation condition using signed-rank test (alpha 0.05). Z-scored activity profiles were obtained for each neuron by subtracting the average firing rate of the neuron across the whole recording from the neuron average activity profile in Hz and dividing it by the SD of the firing rate. The Z-scored activity profiles were then averaged together to generate the population activity profile (Figures 3H–3K). The onset of inhibition (Figures 3Q, S6D, S6E, S9C, and S10D) was measured as the first 2 ms bin after 0 where the cross-correlogram was below 2 SD of a baseline measured in the preceding 50 ms. For Figure S7, type by type comparisons (Figures S7A, S7B, and S7G) were done with Wilcoxon rank-sum test applying Bonferroni correction, leading to an alpha of 0.0083 for Figures S7A and S7B and 0.0125 for Figure S7G. To assess the link between control firing rate, ramp size and photoactivation effect (as defined in Figure S7H), we did a simple linear regression model, photoactivation effect = \alpha ramp size + \beta control firing rate \gamma. In this regression, only \alpha was significantly different from 0 (\alpha = −0.79, p = 1.26e-6, \beta = 0.03, p = 0.76 and \gamma = 2.04, p = 0.08).

Classification of cerebellar cortex and ALM units

Cerebellar cortex units from crus 1 (Figures 4 and 5) and crus 2 (Figure S12) recordings were classified as putative Purkinje cells (PCs) by fitting their interspike intervals distributions (Figure S11B) with a lognormal function. The distribution of means and standard deviations from the log normal fits were then clustered in 2 groups using k-means clustering (Figure S11C). Units belonging to the group

with higher ISIs mean and SD were considered as non-PCs. This group likely comprises inhibitory interneurons found in the molecular layer (Blot et al., 2016; Gao et al., 2012) or in the granule cell layer (Golgi cells) (Gao et al., 2012), but might also contain PCs with low firing rates or PCs whom recording quality deteriorated during the recording session. We nonetheless adopted this conservative measure to avoid contaminating of PCs sample with inhibitory interneurons.

Accurate classification of units as PCs was confirmed by detecting climbing fiber-generated complex spikes (CSs, Figure S11E). For every single unit, we first identified putative PCs by applying a 15 Hz threshold to the baseline firing rate. Next, like previous studies (Blot et al., 2016; Khilkevich et al., 2018; de Solages et al., 2008), we applied analyses that aimed to separate simple and complex spikes based on consistent differences in their typical waveforms. While the exact waveform of complex spikes can vary substantially, a common feature is a presence of positive deflection following the spike peak, to which we will refer as ''late peak.'' For all waveforms belonging to a single unit, we calculated the distribution of late peak values within 3 ms following the spike peak time. Identified waveforms with late peak values larger than 3 median absolute deviations (MAD) of the median late peak value were selected. The mean profile of these waveforms was used as a proxy for putative complex spike waveform. The mean profile of the rest of waveforms resulted in a simple spike waveform. For every spike, we calculated Spearman correlation coefficients between corresponding waveform and the mean waveforms of complex and simple spikes. The combination of: positive correlation with mean complex spike waveform and; a positive difference between correlations with mean complex and simple spike waveforms was used to separate putative complex spikes from simple spikes. Complex spikes were confirmed if their cross-correlogram with simple spikes from the same unit (Figure S11D) exhibited tens of ms-long pauses in SS firing (Figure S11F). In crus 1 (19/72) and in crus 2 (13/56) units classified as PCs exhibited CSs but none classified as non-PCs.

In crus 1 we also confirmed correct unit classifications as PCs if those units had significantly modulated cross-correlograms with ms-latency through with DN units (Figures 4M and 4N). Ten units classified as PCs exhibited such cross-correlograms. Three units classified as non-PCs had similar cross-correlograms with DN units and were integrated in the PC group. In Figures 4, 5, and S12 only putative PCs (72/89 of all units for crus1 and 56/84 for crus 2) are included.

Units were classified as 'fat spikes' (Figure S11G) (Gao et al., 2012) if the full width at half maximum of their spike waveform exceeded 500 ms (Figure S11H). Fat spikes units were considered to exhibit significant increase in spiking probability if the number of spikes in the last 500 ms before reward were significantly lower than in the first 500 ms after reward across trials (p < 0.05, Wilcoxon Rank-sum test; Figures 5I–5M).

ALM units were classified as putative pyramidal neurons or fast-spiking interneurons based on spike width as described in (Guo et al., 2014) and only putative pyramidal neurons were analyzed.

Generalized linear model

We used neuroGLM (https://github.com/pillowlab/neuroGLM) to classify neuronal responses with models obtained from linear regression between external covariates and spike trains in single trials. Spike trains were discretized into 1 ms bins and each external event was represented as follows: running speed was added as a continuous variable. Reward times, lick times, and visual cue times were represented as boxcar functions convolved with smooth temporal basis functions defined by raised cosine bumps separated by $\pi/2$ radians (25 ms). The resulting basis functions covered a -4 to 2 s window centered on reward time, and -2 to 2 s windows for lick and visual cue times. We then computed Poisson regression between spike trains and the basis functions and running speed. The resulting weight vectors were then convolved with event times and linearly fitted with the spike times peri-stimulus time histograms smoothed with a 25 (for lick times) or 50 ms Gaussian (for reward times and running speed) to compute the coefficient of determination for each trial (Figure S2). We divided the fit between reward times model and firing rates in two time windows: -4 to 0 s and 0 to 2 s relative to reward time to differentiate between pre- and post-reward neuronal activity (Figures S2A–S2F). Fits with mean coefficient of determination across trials exceeding 0.17 were selected to classify units (Figure S2K).

Linear modeling of Purkinje cells firing rate from running speed

For each mouse, the running speed was low-pass filtered at 100 Hz and discretized in bins of 5 cm/s from the minimum to the maximum values rounded to the nearest integers. The times of mouse running speed were then sorted according to which bin the running speed fell into and the firing rate of PCs at those times was then extracted and averaged. The resulting PCs firing rates to running speed tuning curves were fit using the MATLAB smoothing spline function. PCs activity models were obtained by converting the running speed from the filtered trace to the corresponding firing rates on the tuning curves fits. For this analysis we included only the PCs that exhibited decreases in firing rates preceding reward times satisfying the following condition: mean(FR[-4,-3]s) > mean(FR[-2,0]s)+2*SD(FR[-4,-3]s), where time in square brackets is relative to reward times.

The averaged modeled firing rates were then subtracted from the averaged PCs firing rates around deceleration events outside of the reward zone ([-2,0]s, mean(DecelModelFR) – mean(DecelPcFR)) and around reward times ([-2,0]s, mean(RewardModelFR) – mean(RewardPcFR)). In most cases the number of reward times exceed that of deceleration events and the former were then grouped in blocks (i) containing the same number of trials than in the latter. Models were considered to overestimate the PCs firing rates around reward times if mean(DecelModelFR)-mean(DecelPcFr) > mean(RewardModelFR)-mean(RewardPcFR(i)) in at least 80% of cases. The plot in Figure 5G shows the mean values across all reward time blocks for the 'Reward' condition (right column).